*buildings*

MDPI

*Article*

# Compressive Behaviour of Circular High-Strength Self-Compacting Concrete-Filled Steel Tubular (CFST) Stub Columns Under Chloride Corrosion: Numerical Simulation

**Jun Zheng [1], Qian Xu [2], Weiwei Wang [1,3,*], Zhiyuan Zheng [4], Mingxun Hou [1] and Xuetao Lyu [4,*]**

[1] School of Architectural Engineering, Guangzhou Vocational University of Science and Technology, Guangzhou 510000, China; zhengjun@gkd.edu.cn (J.Z.); houmingxun@gkd.edu.cn (M.H.)
[2] School of Civil and Architectural Engineering, Liaoning University of Technology, Jinzhou 121001, China; eileenxq2022@163.com
[3] School of Civil Engineering & Transportation, South China University of Technology, Guangzhou 510641, China
[4] School of Civil Engineering and Transportation, Foshan University, Foshan 528000, China; zzy2024196@163.com
* Correspondence: wangweiwei@gkd.edu.cn (W.W.); lxtwww30@fosu.edu.cn (X.L.)

**Abstract:** This paper investigates the strength and behaviour of high-strength self-compacting concrete-filled steel tubular (HSSC-CFST) stub columns under axial compression. HSSC-CFST columns are high-performance structural members with wide applications in engineering structures. Nevertheless, relevant studies have commonly focused on the mechanical performance of HSSC-CFST in indoor environments. A finite element (FE) model was developed to predict the axial load capacity of HSSC-CFST stub columns subjected to chloride corrosion. According to this, several crucial geometric and material parameters were designed to investigate the influences on strength, initial stiffness, and ductile performance. Moreover, the analysis on failure mechanisms was investigated by *N*-ε curves and stress development in the whole loading process. The impacts of key parameters on the reduction factor of axial load capacity were also identified. The numerical analysis results indicate that the axial strength of HSSC-CFST stub columns under chloride corrosion was significantly heightened by increasing the strength of core self-compacting concrete, while contrary results were found with the increase in the steel ratio and yield strength of the steel tube. Lastly, design recommendations for the axially loaded HSSC-CFST were presented by modifying the design codes in CECS104-99. The proposed model is shown to be able to estimate the axial load-bearing capacity of HSSC-CFST stub columns more accurately.

**Keywords:** high-strength self-compacting concrete; concrete-filled steel tubular; chloride corrosion; stub column; axial compressive behaviour

check for updates

**Citation:** Zheng, J.; Xu, Q.; Wang, W.; Zheng, Z.; Hou, M.; Lyu, X. Compressive Behaviour of Circular High-Strength Self-Compacting Concrete-Filled Steel Tubular (CFST) Stub Columns Under Chloride Corrosion: Numerical Simulation. *Buildings* **2024**, *14*, 3775. https://doi.org/10.3390/buildings14123775

Academic Editor: Grzegorz Ludwik Golewski

Received: 20 October 2024
Revised: 23 November 2024
Accepted: 24 November 2024
Published: 26 November 2024

**Copyright:** © 2024 by the authors. Licensee MDPI, Basel, Switzerland. This article is an open access article distributed under the terms and conditions of the Creative Commons Attribution (CC BY) license (https://creativecommons.org/licenses/by/4.0/).

## 1. Introduction

Concrete-filled steel tubular (CFST) columns have been widely used in civil engineering structures, such as high-rise buildings, arch bridges, offshore structures [1–4]. The interaction effects between the steel tube and core concrete induce the superior performance of CFST members [5,6]. Nonetheless, the interaction defects are mainly caused by concrete casting and shrinkage, which weaken the interaction between the steel tube and the concrete [7–11]. The incorporation of self-compacting concrete (SCC), with its high self-drying capacity and pronounced shrinkage, in CFST members is a promising solution to enhance the interaction between the steel tube and concrete, thereby mitigating the defects associated with conventional concrete [12–14].

Extensive research has been conducted on the structural behaviour of CFST columns under axial compression. Han et al. [15] conducted a thorough investigation of 38 high-strength steel (HSS) columns filled with self-compacting concrete (SCC) to evaluate both

their axial and eccentric behaviour. Their findings indicated that the utilization of SCC had a minimal influence on the sectional capacity. In another study, Yu et al. [16] tested 28 high-strength SCC-filled steel tubular columns, revealing that the ductility of these columns was lower compared to normal-strength CFSTs, particularly under axial loading conditions. Han et al. [17] furthered their research by testing 50 stub columns made of structural steel (HSS) filled with SCC under axial compression. They proposed a theoretical model that accounted for the confinement coefficient and found that SCC had a slight effect on the axial compressive load capacity, confirming the applicability of existing design codes.

Mahgub et al. [14] conducted a study on the axial compressive behaviour of self-compacting concrete (SCC)-filled elliptical steel tube columns using three series of specimens. Their findings revealed that the axial compressive strength of these columns increases with an enhancement in the strength of SCC. Ahmed et al. [18] presented a theoretical model that incorporates confinement effects to investigate the axial performance of SCC columns reinforced with steel tubes. The research demonstrated that the axial performance of these columns is influenced by both geometrical and material strength parameters.

Teoh et al. [19] tested 16 lightweight SCC (LWSCC)-filled concrete-filled box-beam-slab (CFBBS) columns and four hollow columns, revealing that the composite action diminishes as the member length increases. Li et al. [20] conducted experiments on 36 concrete-filled steel tube (CFST) columns with concrete strengths ranging from C40 to C60 and varying steel fiber volume percentages of 0%, 0.6%, and 1.2%. Their results showed that the self-stress improved the ultimate load, with an optimal level of 0.10.

Gong et al. [21] both experimentally and numerically examined the seismic performance of recycled steel-confined concrete-filled steel tube (RSCCFST) columns. Their study discovered that the load capacity and ductility of these columns increase with an increase in the reinforcement ratio and steel tube thickness.

It is worth noting that numerous research on the behaviour of SCCFST members mainly focused on their performance in normal environments [22,23]. However, in some practical conditions, CFST members serve in complex service environments, such as offshore water and in-shore corrosive atmosphere. Furthermore, some of these members suffered both axial loading and chloride corrosion, which led to a decrease in the wall-thickness of the outer steel tube. This reduction can significantly impact the confinement effect within the cross-section [24].

Several studies have reported on the performance of CFST members considering the chloride corrosion environment. Han et al. [24] and Hou et al. [25] studied CFST columns and beams by experimental study and numerical study, and indicated that chloride corrosion had a significant effect on the mechanical behaviour and that CFST members presented a ductile manner. Furthermore, the ultimate strength could be reflected by the variations of confinement coefficient.

Han et al. [26] further delved into the mechanical behaviour of circular CFST stub columns subjected to sustained load and chloride corrosion. Their findings highlighted the significant impact of chloride corrosion on the ultimate compressive strength, resulting in decreased section diameter, weakened steel confinement, and deteriorated steel material.

Hou et al. [27] established a FEA model for investigating the life-cycle performance of CFST columns, with consideration of the effects of chloride corrosion. It was revealed that the combined effects of sustained load and corrosion led to a notable reduction in axial load capacity.

Li et al. [28] conducted series tests on CFDSTs filled with seawater and sea sand concrete under axial compression. It was found that the ultimate strength and post-peak behaviour were mainly affected by the confinement factor. Hua et al. [29] tested 11 beam-columns under 120-day sustained load and chloride corrosion, observing that corrosion had a more pronounced negative impact on mechanical behaviour than sustained load alone, particularly under bending load. Additionally, Hua et al. [30] numerically studied the behaviour of square CFST beam-columns under corrosion, concluding that the

ultimate strength of CFST columns under chloride corrosion is mainly determined by the confinement factor.

Guo et al. [31] tested 15 specimens with artificial notch to investigate the effects of local corrosion on square CFST under axial compression. Their findings showed that the horizontal notches significantly reduced compression strength, while narrow vertical notches had a minor impact. The compression strength is primarily governed by the effective cross-sectional area of the steel tube.

The aforementioned studies have highlighted the benefits of utilizing both high-strength concrete and self-compacting concrete in CFST columns subjected to chloride corrosion. Chloride corrosion leads to the reduction of steel tube wall-thickness and decreased confinement effect, which result in a tendency for the axial load to transfer from the steel tube to the core concrete. Therefore, it is necessary to conduct research on the performance of axially loaded circular CFST stub columns constructed with high-strength self-compacting concrete.

In this paper, numerical analysis models were attempted to be established to investigate the performance of axially loaded high-strength self-compacting concrete-filled steel tubular stub columns subjected to chloride corrosion. Based on the assumption of reduction in wall-thickness of the steel tube and the successful validation of FE models by previous test results, a comprehensive series of parametric studies were presented. The behaviour of axially loaded HSSC-CFST stub columns subjected to chloride corrosion was studied in terms of various parameters, including section diameter, steel ratio, compressive strength of core concrete, and yield strength of the steel tube. Further research will be conducted on the standard dry plates method [32] of experimental tests and FE model considering the reference time of chloride diffusion [33].

In addition, the failure modes, axial load versus deformation curves, axial load versus axial strain curves, and longitudinal stress development of core concrete and steel tube were discussed in detail. To predict the designed axial compressive strengths of HSSC-CFST stub columns, a reduction factor is introduced alongside a design formula in accordance with the specifications outlined in CECS104-99 [34].

## 2. Finite Element Simulation and Validation

### *2.1. General*

The software ABAQUS 6.14/Standard was employed to create the present FE (Finite Element) model for investigating the structural behaviour of circular high-strength self-compacting concrete-filled steel tubular stub columns subjected to varying corrosion rates. Representative FE models for HSSC-CFST stub columns are illustrated in Figure 1. Subsequently, these FE models were validated against experimental data to ensure their accuracy.

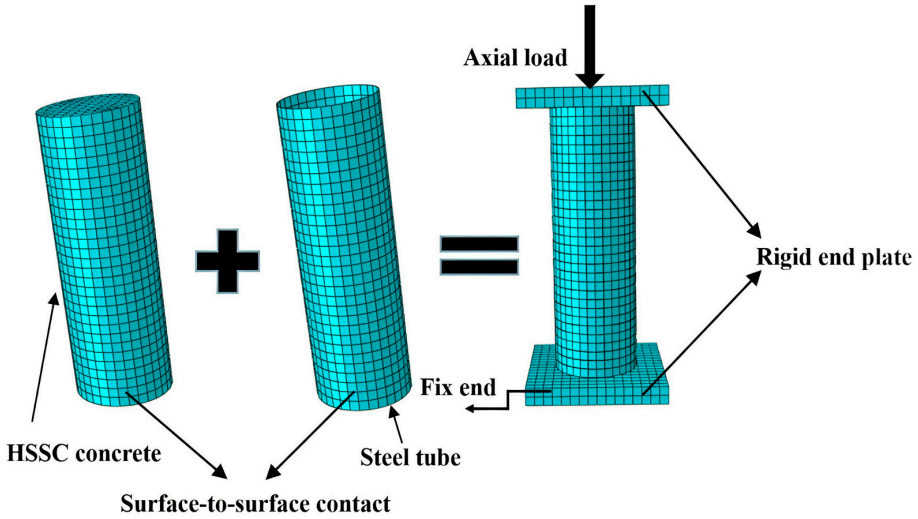



**Figure 1.** Typical models for HSSC-CFST stub columns in ABAQUS.

### 2.2. Finite Element Type and Mesh

Depicted in Figure 1 is the FE model for the HSSC-CFST stub column incorporating top and bottom discrete rigid end plates. A reference point (RP) was set at the center of each end plate with RP1 and RP2 designated for the application of loads and boundary restraints, respectively. C3D8R and S4R were adopted for the core high-strength self-compacting concrete and the steel tube, respectively. It should be noted that mesh sensitivity analysis was undertaken to ensure the optimal mesh size, which balanced accuracy and computational efficiency. It indicated that a mesh size of $D/10$ can achieve this balance. The typical mesh configuration for the high-strength SCCFST stub columns is shown in Figure 1.

### 2.3. Interaction Between Components

The Coulomb Friction Model was employed to imitate the general bond strength in tangential contact behaviour. In the surface-to-surface contact option, the steel tube was designated as the slave surface while the core high-strength self-compacting concrete surface was chosen as the master surface. The friction coefficient between the steel tube and the HSSC concrete was considered to be 0.6, as suggested by Yu et al. [35]. The ultimate shearing stress was fixed at 0.4 MPa [36]. Additionally, the surface-based interactions were also implemented between the end plates and the core HSSC concrete. Moreover, the top and bottom end plates were interconnected with steel tubes through a "Tie" constraint, ensuring that the end plates maintained identical displacements and rotations throughout the entire loading process.

### 2.4. Stress-Strain Relationships for Different Materials

#### 2.4.1. Steel Tube in Compression and Tension

The stress-strain model for steel utilized in numerical simulations was formulated utilizing the elastic–plastic model. The compression and tension behaviours can be expressed through five-stage constitutive laws. In the simulation of high-strength HSSC-CFST stub columns subjected to chloride corrosion, the stress–strain model proposed by Han [37] was employed, which is represented by

$$\sigma_s = \begin{cases} E_s\varepsilon_s & \varepsilon_s < \varepsilon_e \\ -A\varepsilon_s^2 + B\varepsilon_s + C & \varepsilon_e < \varepsilon_s \le \varepsilon_{e1} \\ f_y & \varepsilon_{e1} < \varepsilon_s \le \varepsilon_{e2} \\ f_y[1 + 0.6(\varepsilon_s - \varepsilon_{e2})/(\varepsilon_{e3} - \varepsilon_{e2})] & \varepsilon_{e2} < \varepsilon_s \le \varepsilon_{e3} \\ 1.6f_y & \varepsilon_s > \varepsilon_{e2} \end{cases} \quad (1)$$

in which $\sigma_s$ stands for the steel stress, $\varepsilon_s$ represents the strain, $E_s$ and $f_y$ denote the elastic modulus and yield strength of steel, $\varepsilon_e$ corresponds the strain corresponding to the stress of $f_p$, which is taken as $\varepsilon_e$=0.8$f_y/E_s$, $\varepsilon_{e1}$ is taken as $\varepsilon_{e1}$ = 1.5$\varepsilon_e$, $\varepsilon_{e2}$ is taken as $\varepsilon_{e2}$ = 10$\varepsilon_{e1}$, and $\varepsilon_{e3}$ is taken as $\varepsilon_{e3}$ = 100$\varepsilon_e$.

In Equation (1), A, B, and C are parameters, which are mathematically derived by strains and expressed by

$$A = 0.2f_y(\varepsilon_{e1} - \varepsilon_e)^2 \quad (2)$$

$$B = 2A\varepsilon_{e1} \quad (3)$$

$$C = 0.8f_y + A\varepsilon_e^2 - B\varepsilon_e \quad (4)$$

It should be mentioned that chloride corrosion has led to the deterioration of the steel tube. Therefore, for steel tubes subjected to chloride corrosion, the elastic modulus and yield strength of them were adopted by the modified equations in Ref. [38], especially for Q345 steel with corrosion rate ranges from 0% to 30%, which were expressed as follows:

$$E_{se} = (1 - 0.537\gamma)E_s \quad (5)$$

$$f_{ye} = (1 - 0.676\gamma)f_y \quad (6)$$

where $\gamma$ is the chloride corrosion rate ($\gamma = t/t_0 \times 100\%$), $t_0$ and $t$ stand for the initial and corroded thicknesses of the steel tube, respectively, and $E_{se}$ and $f_{ye}$ denote the elastic modulus and yield strength of the steel tube subjected to chloride corrosion.

#### 2.4.2. Concrete in Compression

Studies on CFST columns constructed with self-compacting concrete have proven that their strength is comparable to that of normal CFST specimens [15,17]. Thus, the concrete compressive model employed in high-strength self-compacting CFST stub columns was adopted the model proposed by Han et al. [35], as outlined in Equations (7)–(17).

$$y = 2x - x^2 \qquad (x \le 1) \tag{7}$$

$$y = \begin{cases} 1 + q\left(x^{0.1\xi} - 1\right) & \xi \ge 1.12 \\ \frac{x}{\beta(x-1)^2 + x} & \xi < 1.12 \end{cases} \qquad (x > 1) \tag{8}$$

$$x = \frac{\varepsilon}{\varepsilon_0} \tag{9}$$

$$y = \frac{\sigma}{\sigma_0} \tag{10}$$

$$\sigma_0 = \left[1 + \left(-0.054\xi^2 + 0.4\xi\right) \cdot \left(\frac{24}{f_c'}\right)^{0.45}\right] \cdot f_c' \tag{11}$$

$$\varepsilon_0 = \varepsilon_{cc} + \left[1400 + 800\left(\frac{f_c'}{24} - 1\right)\right] \cdot \xi^{0.2} \quad (\mu\varepsilon) \tag{12}$$

$$\varepsilon_{cc} = 1300 + 12.5 \cdot f_c' \quad (\mu\varepsilon) \tag{13}$$

$$q = \frac{\xi^{0.745}}{2 + \xi} \tag{14}$$

$$\beta = \left(2.36 \times 10^{-5}\right)^{[0.25 + (\xi - 0.5)^7]} \cdot f_c' \cdot 3.51 \times 10^{-4} \tag{15}$$

$$\xi = \frac{A_s f_y}{A_c f_{ck}} = \alpha_s \frac{f_y}{f_{ck}} \tag{16}$$

$$\alpha_s = \frac{A_s}{A_c} \tag{17}$$

in which $f_c{}'$ is the concrete cylinder strength ($f_c{}' = 0.8 f_{cu}$, where $f_{cu}$ denotes the concrete cubic strength), $f_{ck}$ is characteristic concrete strength ($f_{ck} = 0.67 f_{cu}$), $\sigma_0$ and $\varepsilon_0$ correspond to the ultimate stress and ultimate strain of core HSSCC, $\zeta$ stands for confinement coefficient, $\alpha_s$ represents the steel ratio, and $A_s$ and $A_c$ are the cross-section area of the steel tube and core HSSCC, respectively.

A modified set of equations considering the effects of chloride corrosion was put forward by Chen et al. [39], expressed by:

$$\alpha_e = A_{se}/A_c \tag{18}$$

$$\xi_e = \frac{A_{se} f_{ye}}{A_c f_{ck}} = \alpha_e \frac{f_{ye}}{f_{ck}} \tag{19}$$

$$A_{se} = \pi D(1 - \gamma)t \tag{20}$$

where $A_{se}$ is the area of the steel tube after chloride corrosion, and $t_0$ is the thickness of the steel tube before chloride corrosion.

2.4.3. High-Strength Self-Compacting Concrete in Tension

The core of high-strength steel concrete composite (HSSCC) circular columns may potentially be subjected to tension under chloride corrosion. The stress–strain model, as originally proposed by Han et al. [37] is expressed by

$$y = \begin{cases} 1.2x - 0.2x^6 & x \le 1 \\ \frac{x}{0.31\sigma_p^2(x-1)^{1.7}+x} & x > 1 \end{cases} \quad (21)$$

$$x = \frac{\varepsilon_c}{\varepsilon_p} \quad (22)$$

$$y = \frac{\sigma_c}{\sigma_p} \quad (23)$$

$$\sigma_p = 0.26 \times \left(1.25 f_c'\right)^{\frac{2}{3}} \quad (24)$$

$$\varepsilon_p = 43.1\sigma_p \quad (\mu\varepsilon) \quad (25)$$

where $\sigma_p$ stands for the ultimate concrete tensile stress, and $\varepsilon_p$ is the corresponding strain.

2.4.4. Analysis Parameters

In this paper, the CDP (Concrete Damaged Plasticity) model is applied to characterize the constitutive behaviour of core high-strength self-compacting concrete. A Poisson's ratio of 0.2 was used, and the modulus of elasticity of the concrete was specified according to ACI318-11 [40] as

$$E_c = 4700\sqrt{f_c'} \quad (26)$$

The dilation angle, the ratio of the strength in the triaxial state [41], and the *K* parameter were expressed by

$$\psi = \begin{cases} 56.3 \times (1 - \xi) & \xi \le 0.5 \\ 6.672 \times e^{\frac{7.4}{4.64+\xi}} & \xi > 0.5 \end{cases} \quad (27)$$

$$K_c = \frac{5.5}{5 + 2 \times \left(f_c'\right)^{0.075}} \quad (28)$$

$$f_{b0}/f_{c0} = 1.5 \times \left(f_c'\right)^{-0.075} \quad (29)$$

The eccentricity and the viscosity parameter were taken as 0.1 and 0.0005, respectively.

As depicted in Figure 1, the chloride-corroded high-strength self-compacting CFST stub columns were subjected to axial loading through the end plate. As for the bottom end plate, all displacements and rotations in various directions were effectively constrained (U1 = U2 = U3 = UR1 = UR2 = UR3 = 0). Conversely, for the top end plate, the rotations in three directions were restrained while the displacement in z axis was permitted (U1 = U2 = UR1 = UR2 = UR3 = 0). Tie constraints were used to affix the end plates to the column. A displacement control method was applied to the load deflection analysis of the high-strength self-compacting CFST stub columns, which was specified as $L/10$.

*2.5. Validation of the Current FE Model*

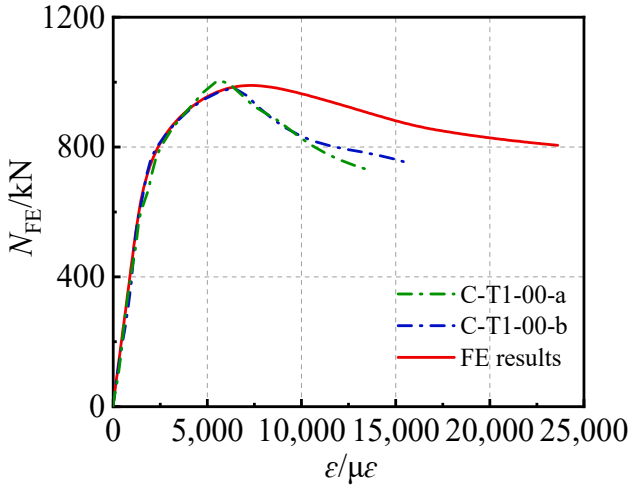
The experimental results obtained by Zheng et al. [42] and Li et al. [43] on axially loaded circular high-strength self-compacting CFST stub columns under chloride corrosion were adopted to verify the FE model. The axial compressive strength of the columns obtained from the experiments ($N_{u,T}$) are compared with the specimens calculated by FE ($N_{u,FE}$) analyses in Table 1. It can be seen that there is a good agreement between the test and FE results, evidenced with a mean value of 0.9994, illustrating the accuracy of the FE model in predicting the ultimate axial compressive strength. Moreover, the coefficient of

variation value of 0.0027, which is close to zero, indicates less scatter in the prediction of ultimate axial compressive strength.

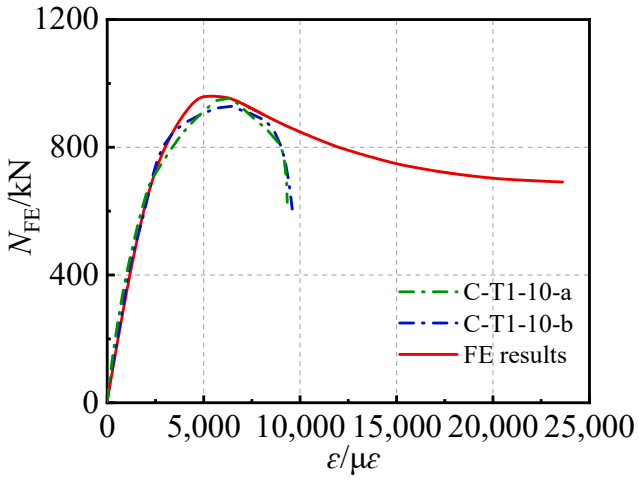
**Table 1.** Comparison of ultimate axial compressive strength between test results and FE results.

| Specimens | $N_{u,T}$ (kN) | $N_{u,FE}$ (kN) | $N_{u,T}/N_{u,FE}$ | Specimens | $N_{u,T}$ (kN) | $N_{u,FE}$ (kN) | $N_{u,T}/N_{u,FE}$ |
|---|---|---|---|---|---|---|---|
| C-T1-00-a | 985.2 | 1012.4 | 0.973 | C-T2-10-b | 1134.8 | 1123.6 | 1.010 |
| C-T1-00-b | 1020.1 | 1012.4 | 1.008 | C-T2-20-a | 936.4 | 1044.9 | 0.896 |
| C-T1-10-a | 937.1 | 961.9 | 0.974 | C-T2-20-b | 1016.4 | 1044.9 | 0.973 |
| C-T1-10-b | 963.5 | 961.9 | 1.002 | C-T3-00-a | 1323.3 | 1410.1 | 0.938 |
| C-T1-20-a | 843.6 | 883.6 | 0.955 | C-T3-00-b | 1421.9 | 1410.1 | 1.008 |
| C-T1-20-b | 898.3 | 883.6 | 1.017 | C-T3-10-a | 1339.4 | 1288.9 | 1.039 |
| C-T2-00-a | 1140.7 | 1233.8 | 0.925 | C-T3-10-b | 1314.2 | 1288.9 | 1.020 |
| C-T2-00-b | 1225.2 | 1233.8 | 0.993 | C-T3-20-a | 1266.8 | 1167.7 | 1.085 |
| C-T2-10-a | 1140.5 | 1123.6 | 0.983 | C-T3-20-b | 1304.3 | 1167.7 | 1.117 |
| C-114-5 | 459.1 | 426.2 | 1.077 | C-114-15 | 364.3 | 353.0 | 1.032 |
| C-114-10 | 372.3 | 386.7 | 0.963 | C-114-20 | 341.6 | 323.7 | 1.055 |
| C-114-25 | 269.1 | 285.5 | 0.943 | | | | |
| | | | Mean Value | | | | 0.9994 |
| | | | COV | | | | 0.0027 |

The axial strain ($\varepsilon$)-axial load ($N$) curves obtained both from experimental and FE results are shown in Figure 2. Evidently, the $\varepsilon$-$N$ curves calculated by FE models have a good agreement with the ones obtained from test results, particularly in terms of the initial stiffness and ultimate axial compressive strength. Nevertheless, the descending stages of the curve simulated by FE models were with some deviations from the experimental results. This part of the curve is determined by Equation (8), where the used parameters are related to the area of core concrete, steel tube, the shape, and residual strength. These parameters cannot be directly controlled by the confinement coefficient, due to the influence of chloride corrosion. Therefore, the descending branches of curves match well with experimental results such as C-T2-00-a, C-T2-10-a, C-T3-00-a/b, and C-T3-10-a/b, whereas specimens such as C-114-5 and C-114-10 exhibit less congruence with the test data.

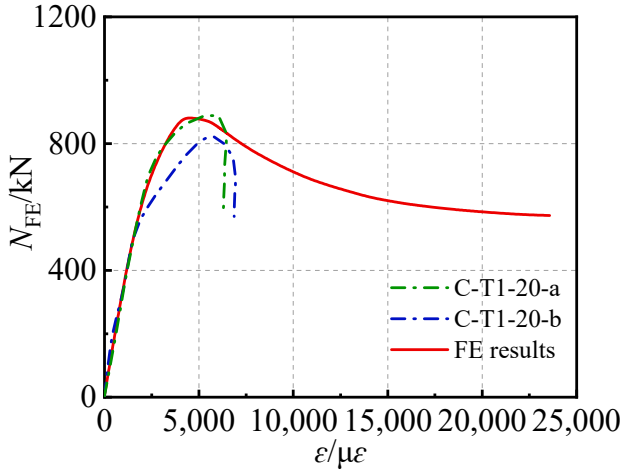



(**a**) C-T1-00

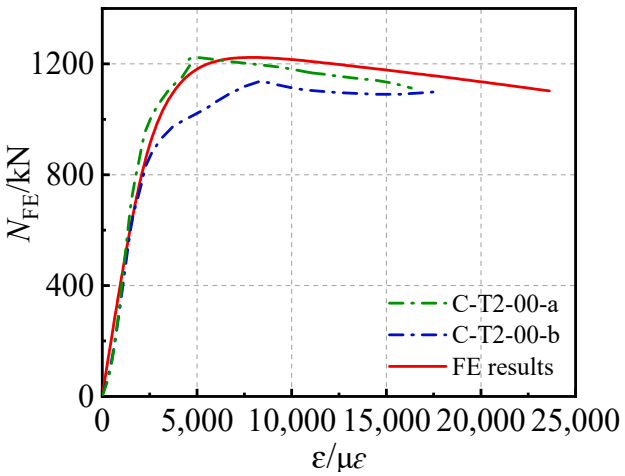



(**b**) C-T1-10

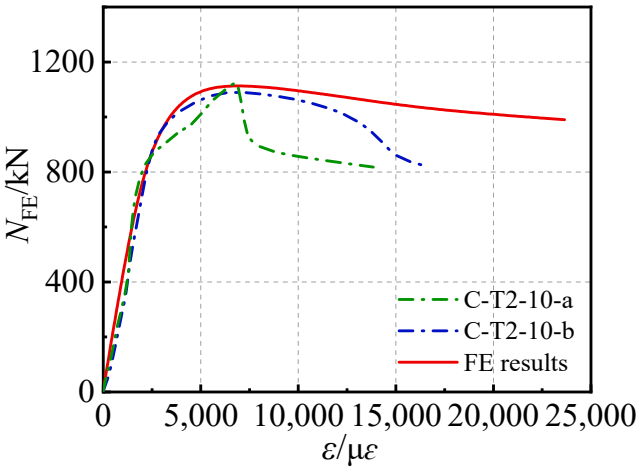
**Figure 2.** *Cont.*



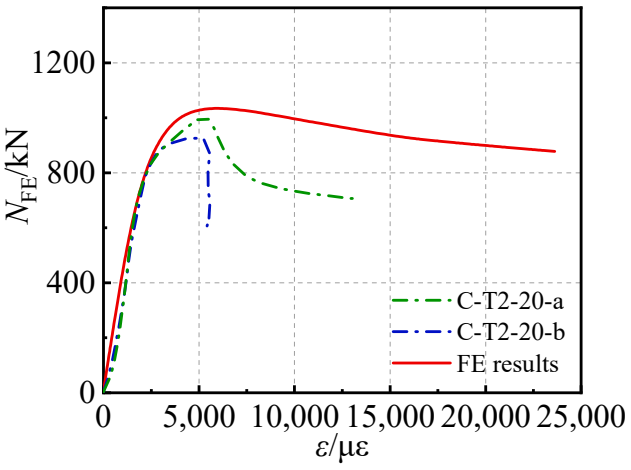

(**c**) C-T1-20



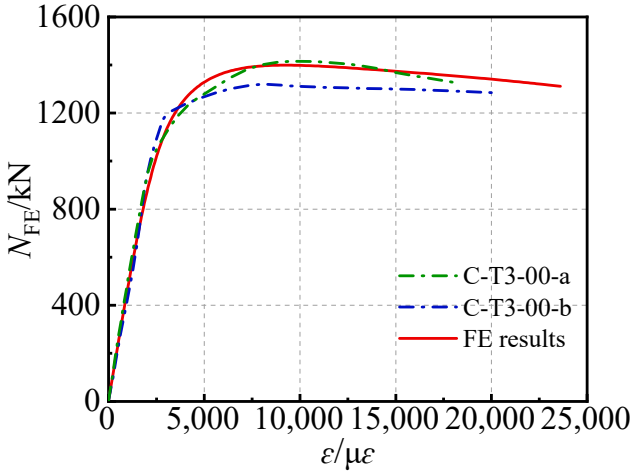

(**d**) C-T2-00



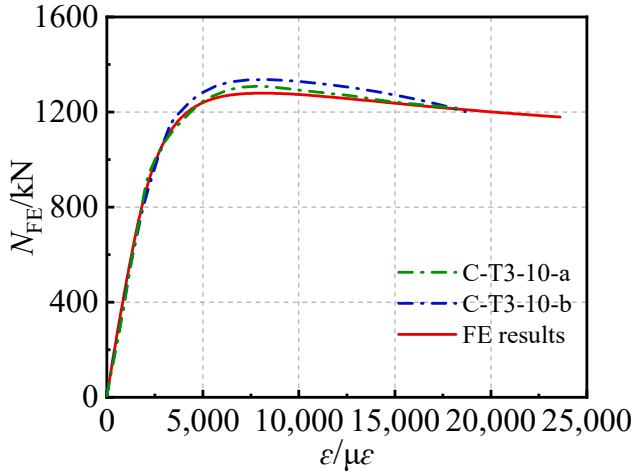

(**e**) C-T2-10




(**f**) C-T2-20

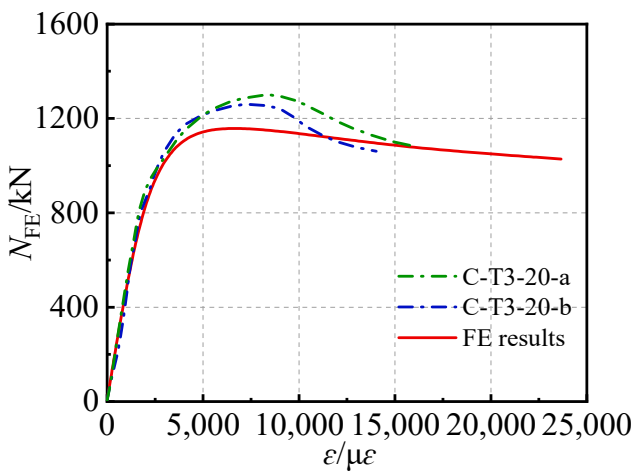



(**g**) C-T3-00

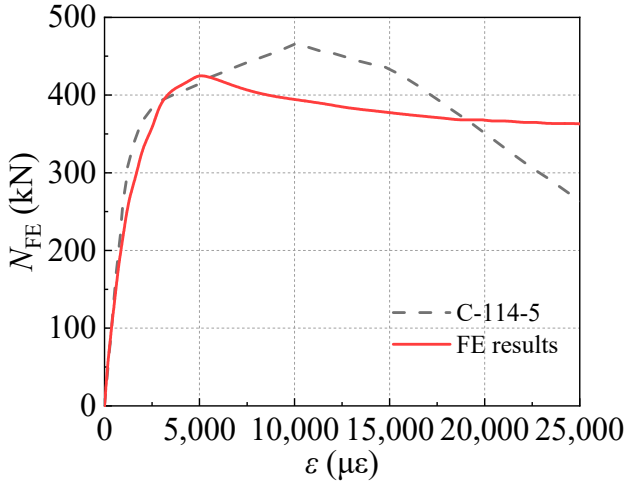



(**h**) C-T3-10

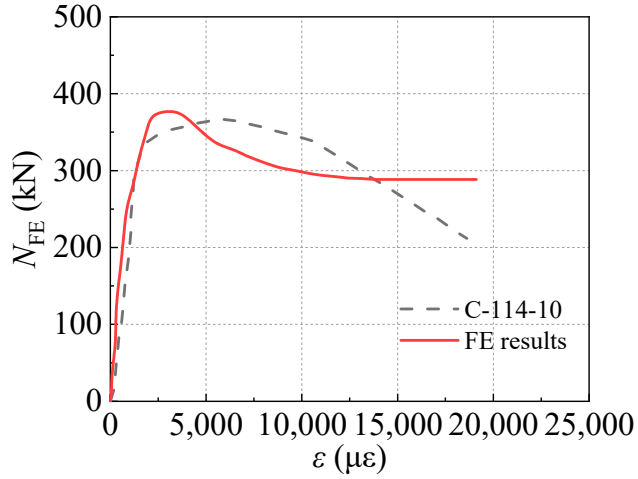
**Figure 2.** *Cont.*



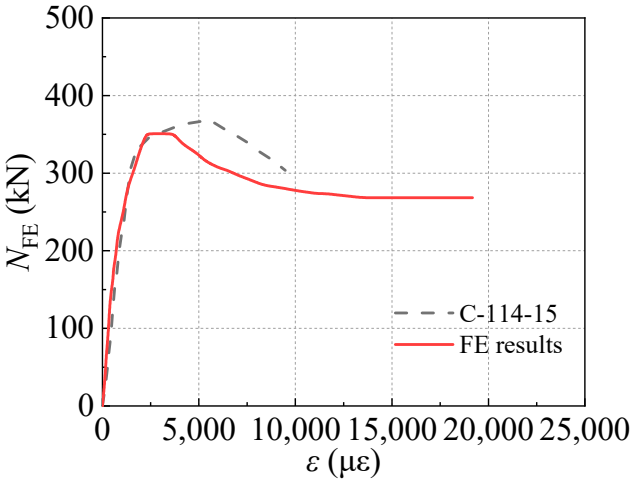

(**i**) C-T3-20



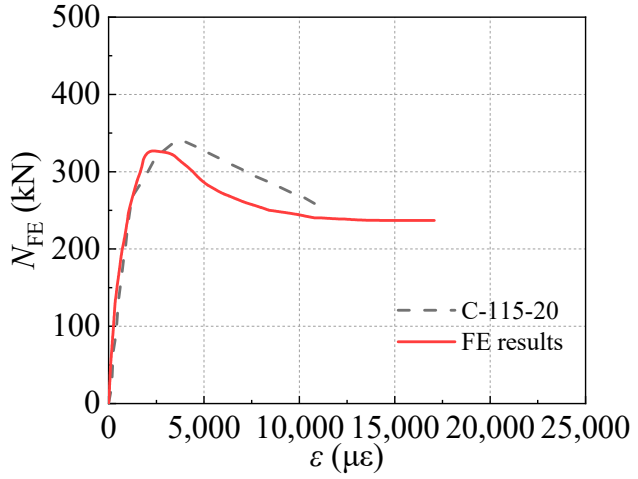

(**j**) C-114-5



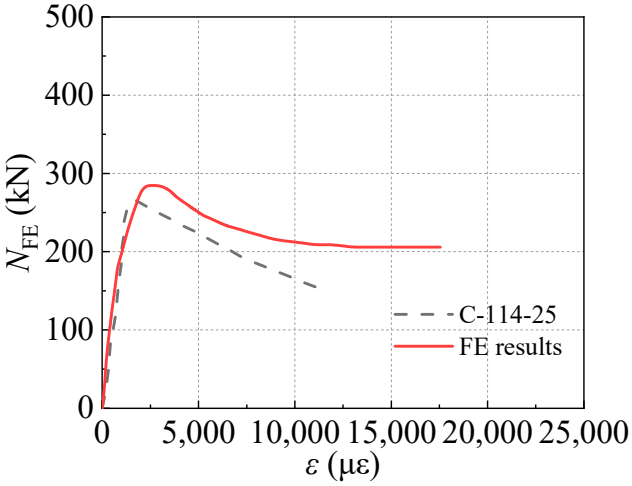

(**k**) C-114-10




(**l**) C-114-15




(**m**) C-114-20




(**n**) C-114-25

**Figure 2.** Comparison between the FE model and test results of axial load versus longitudinal strain.

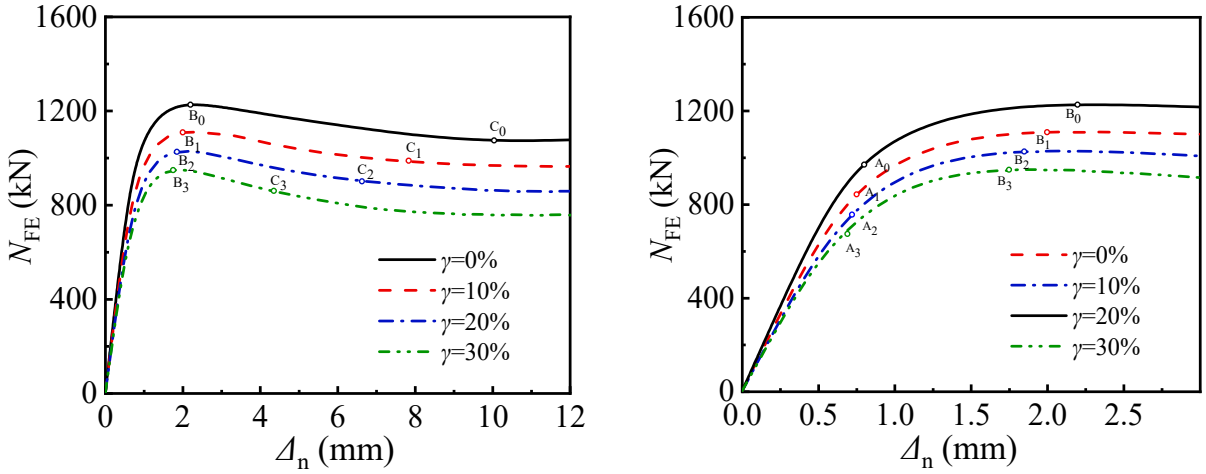
The negligible disparity between the FE model and test results arises from the occasional uncertainties inherent in the actual material properties, imperfections, and site conditions. As depicted in Figure 2, the FE model accurately captures the correlation

between axial load and strain. Furthermore, the FE model presented in this paper effectively represents the behaviour of HSSC-CFST stub columns subjected to chloride corrosion.

## 3. Structural Behaviour

### *3.1. Axial Load Versus Axial Deformation Relationships*

To clarify the failure mechanism of high-strength self-compacting CFST stub columns subjected to chloride corrosion, the failure response of typical columns under such conditions, as derived from finite element analysis, is presented as an illustrative example in Figure 3.




(**a**) NFE-Δn curve (**b**) partial enlarged curve

**Figure 3.** Axial load versus axial deformation in the whole compression process: (**a**) $N_{FE}$-$\Delta_n$ curve; (**b**) partial enlarged curve. Note: $A_0$–$A_3$, $B_0$–$B_3$, $C_0$–$C_3$ represents the characteristic points corresponding to corrosion rate of 0%, 10%, 20%, and 30%, respectively.

Figure 3 depicts the axial load versus axial deformation behaviour of the specimens at key points A, B, and C, spanning three distinct stages: the elastic stage (OAi), the elastic–plastic stage (AiBi), and the failure stage (BiCi). Notably, O denotes the initial load point of the specimen, point A aligns with the yield point of the steel tube ($\Delta_{Ai}$, $N_{Ai} = f_y$), point B corresponds to the peak load of the columns ($\Delta_{Bi}$, $N_{Bi} = N_u$), and point C signifies the instant when the axial strength reaches 85% of the peak load during the descending portion of the curve ($\Delta_{Ci}$, $N_{Ci} = 0.85N_u$).

In the elastic (OAi) stage, the axial load for specimens with different chloride corrosion changes linearly with the increasing axial deformation, indicating that the steel tube and core HSSCC carried the axial load independently. Due to minimal lateral deformation, there is no confinement between the steel tube and core concrete. As depicted in Figure 3b, the initial stiffness of specimens subjected to higher levels of chloride corrosion diminishes, leading to an earlier transition into the elastic–plastic stage. Specifically, the axial load corresponding to point A decreases by 13.12%, 22.12%, and 30.59% when the corrosion rate increases from 0% to 10%, 20%, and 30%, respectively. Furthermore, the axial deformation decreases by 6.25%, 10.00%, and 13.75% as the corrosion rate escalates from 0% to 10%, 20%, and 30%, respectively.

In the elastic-plastic (AiBi) stage, the steel tube commences yielding upon the axial load attaining point A. Both axial and lateral strain increase rapidly, signifying an increase in confinement effects. The core high-strength self-compacting concrete transitions into a triaxial state owing to the restraint imposed by the steel tube. Notably, the ultimate axial compressive strength decreases and prematurely enters a descending phase, earlier due to the chloride corrosion. The ultimate compressive strength decreases by 9.60%, 16.36%, and 22.71% with the corrosion rate of 10%, 20%, and 30% compared to the counterpart specimen with a corrosion rate of 0%. Similarly, the axial deformation decreases by 9.09%,

15.91%, and 20.45%, respectively, with the corrosion rate increasing from 0% to 10%, 20%, and 30%.

In the failure stage (BiCi, descending branch of the $N$-$\Delta_n$ curve), the axial compressive strength undergoes a gradual decline with the increasing axial deformation, indicating that the specimen is with good ductility. Failure of the columns is marked by the crushing of core concrete, concurrent with the yielding of the steel tube. Since the thickness and mechanical properties deteriorate with the increasing chloride corrosion rate, it can be seen that the columns decrease more significantly with the increasing corrosion rate, due to the weakened confinement effect of the steel tube. Specifically, the axial compressive strength at point C decreases by 8.02%, 16.20%, and 19.98% as corrosion rate increases from 0% to 10%, 20%, and 30%, respectively. Conversely, the corresponding axial deformation decreases by 21.96%, 34.00%, and 19.98%.

### *3.2. Axial Stress Versus Strain Analysis*

The axial load–strain curves of core concrete and the steel tube were individually examined via strip analysis, as shown in Figure 4. It can be seen that the load-bearing capacity of the steel tube gradually decreases with the corrosion rate, since the chloride ions weaken the thickness and strength of the steel tube. The axial load shares by the steel tube when the stub column attains peak load contributed to 0.395, 0.363, 0.326, and 0.222, respectively, corresponding to a corrosion rate of 0%, 10%, 20%, and 30%. Moreover, the axial load of the steel tube decreases by 8.1%, 17.5%, and 41.3% as the corrosion rate increases from 0% to 10%, 20%, and 30%. On the contrary, the axial load carried by the core concrete increases by 5.3%, 11.4%, and 28.6%. This indicates that chloride corrosion has an obvious effect on the load distribution of the specimen.

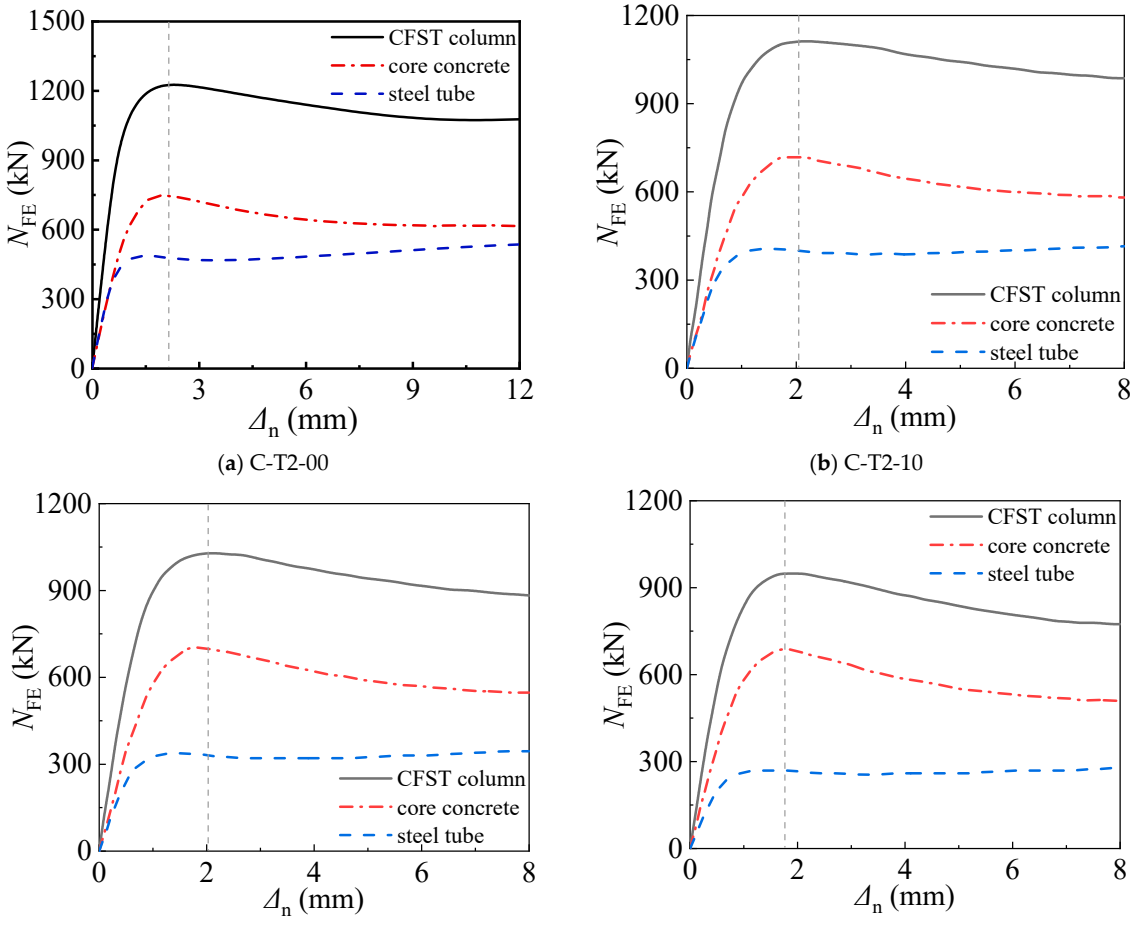


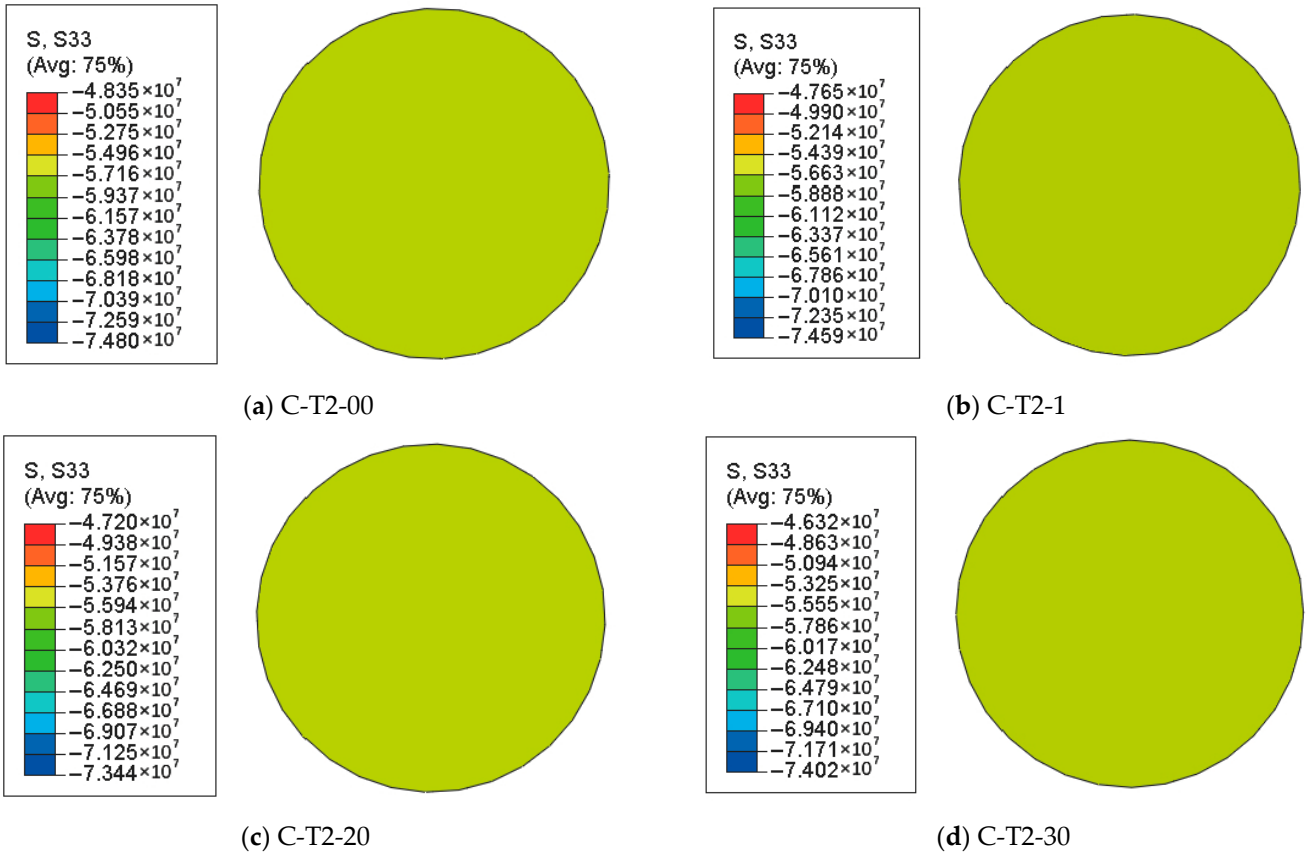

**Figure 4.** Axial load–displacement curve of the concrete and steel tube.

For the stub columns herein, all steel tubes and core concrete components carry the axial compression load throughout the entire loading process, with the core high-strength self-compacting concrete contributing a major portion of the axial resistance. The axial strength carried by the whole specimen decreases, while the load of the steel tube increases due to the confinement effect.

### *3.3. Stress Development*

#### 3.3.1. Core Concrete in the Mid-Height Section

Figures 5–7 represent the S33 stress distribution of HSSC-CFST stub columns at distinct characteristic loading stages (point Ai, Bi, and Ci) with different chloride corrosion rates in the mid-height section. At the end of the elastic stage, the longitudinal stress distributes uniformly in the whole section. The stresses of the columns are in the range of 57.16–59.37 MPa, 56.63–58.88 MPa, 55.94–58.13 MPa, and 55.55–57.86 MPa, respectively, corresponding to the corrosion rate of 0%, 10%, 20%, and 30%. The average longitudinal stresses are 58.27 MPa, 57.76 MPa, 57.04 MPa, and 56.71 MPa, which indicate that the core high-strength self-compacting concrete are in the elastic stage. The average longitudinal stress decreases by 0.88%, 2.11% and 2.68% when the corrosion rate increases from 0% to 10%, 20%, and 30%. This indicates a slight impact of chloride corrosion on longitudinal stress during the elastic phase.




(**a**) C-T2-00 (**b**) C-T2-1

(**c**) C-T2-20 (**d**) C-T2-30

**Figure 5.** Longitudinal stress distribution of core concrete with different chloride corrosion rates in the mid-height section at point A.

At the terminal stage of the elastic–plastic stage, point B (peak load), the longitudinal stresses are in the range of 98.79–105.1 MPa, 95.86–102.3 MPa, 91.87–98.32 MPa, and 89.26–94.36 MPa. At point B, the average stresses are 101.95 MPa, 99.08 MPa, 95.10 MPa, and 91.81 MPa corresponding to the corrosion rate of 0%, 10%, 20%, and 30% within the mid-height section. Compared to point A, the stresses at point B exhibit a notable increase of 43.68 MPa, 41.33 MPa, 38.06 MPa, and 37.66 MPa, respectively. This illustrates that at

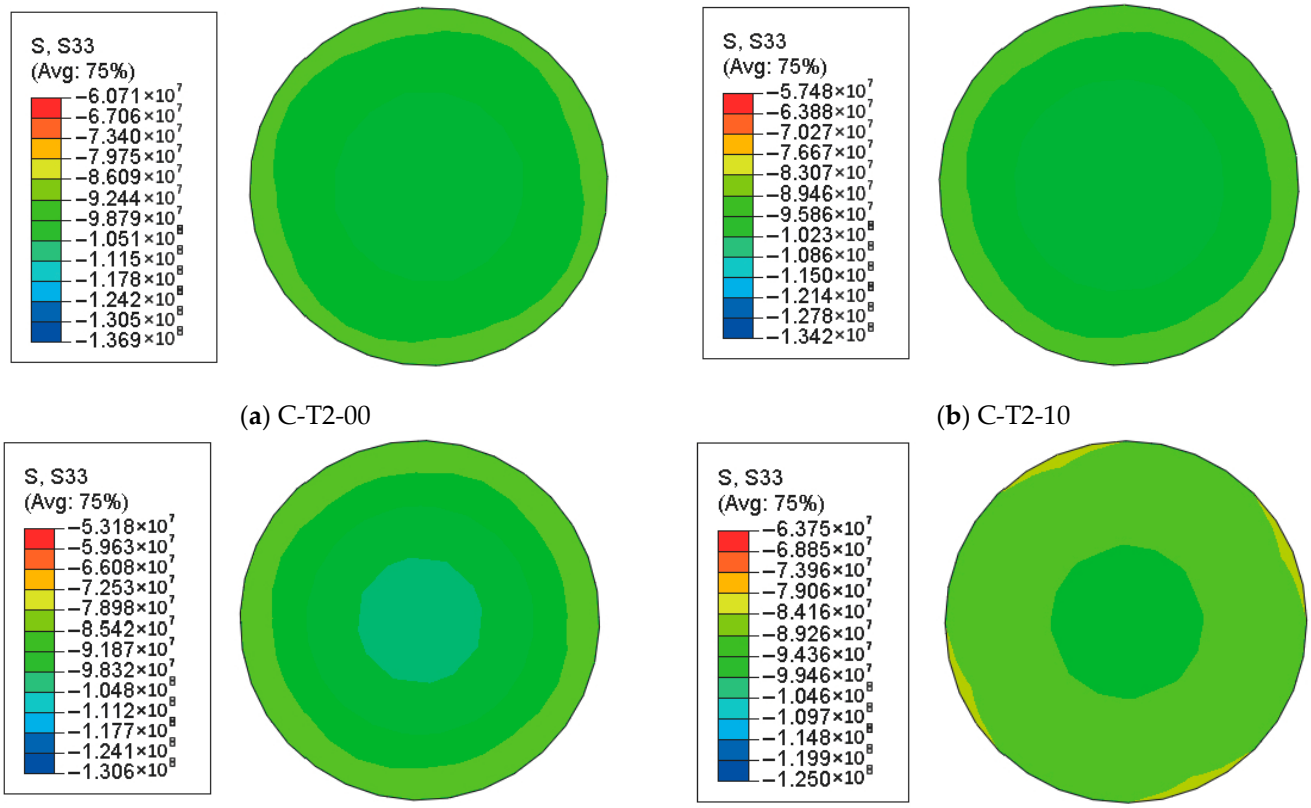
peak load, the lateral deformation was restrained by the steel tube, which causes the core high-strength self-compacting concrete under trial compression. The confinement effect is quite pronounced in the elastic–plastic stage.

As shown in Figure 6, the maximum stress occurs in the center region and decreases sequentially toward the periphery of the section in a circular pattern. This pattern suggests a heightened confinement effect in the central region. The longitudinal stresses decrease by 2.81%, 6.72%, and 9.94% with the corrosion rate increasing from 0% to 10%, 20%, and 30%. The higher the corrosion rate, the larger of the confinement effect. This is due to the deterioration of the steel tube properties induced by chloride corrosion, which weaken the confinement effect of the steel tube.

Figure 7 shows the longitudinal stresses at point C in the mid-height section. The stresses of the columns are in the range of 77.59–86.64 MPa, 73.19–83.12 MPa, 70.17–79.85 MPa, and 64.93–73.16 MPa with the corrosion rate of 0%, 10%, 20%, and 30%. The average values of the longitudinal stress are 82.12 MPa, 78.16 MPa, 75.01 MPa, and 69.05 Mpa, respectively. Compared with those values at point B, the longitudinal stresses decrease by 19.83 MPa, 20.93 MPa, 20.09 MPa, and 22.77 MPa. It indicates that the steel tube still has a confinement effect on the core high-strength self-compacting concrete despite the HSSCC already being crushed. The columns present good ductility. The longitudinal stress decreases by 4.82%, 8.65%, and 15.92% as the corrosion rate increases from 0% to 10%, 20%, and 30%.

According to the stress development of the specimens, it illustrates that the chloride corrosion has a significant effect on the axial stress in the descending stage, then peak load, while having a slight effect on the elastic stage.

Based on the stress progression observed in the specimens, it is evident that chloride corrosion exerts a notable influence on the axial stress during the descending phase, and subsequently impacts the peak load, whereas its effect on the elastic stage is relatively minor.




(**a**) C-T2-00 (**b**) C-T2-10

(**c**) C-T2-20 (**d**) C-T2-30

**Figure 6.** Longitudinal stress distribution of core concrete with different chloride corrosion rates in the mid-height section at point B.

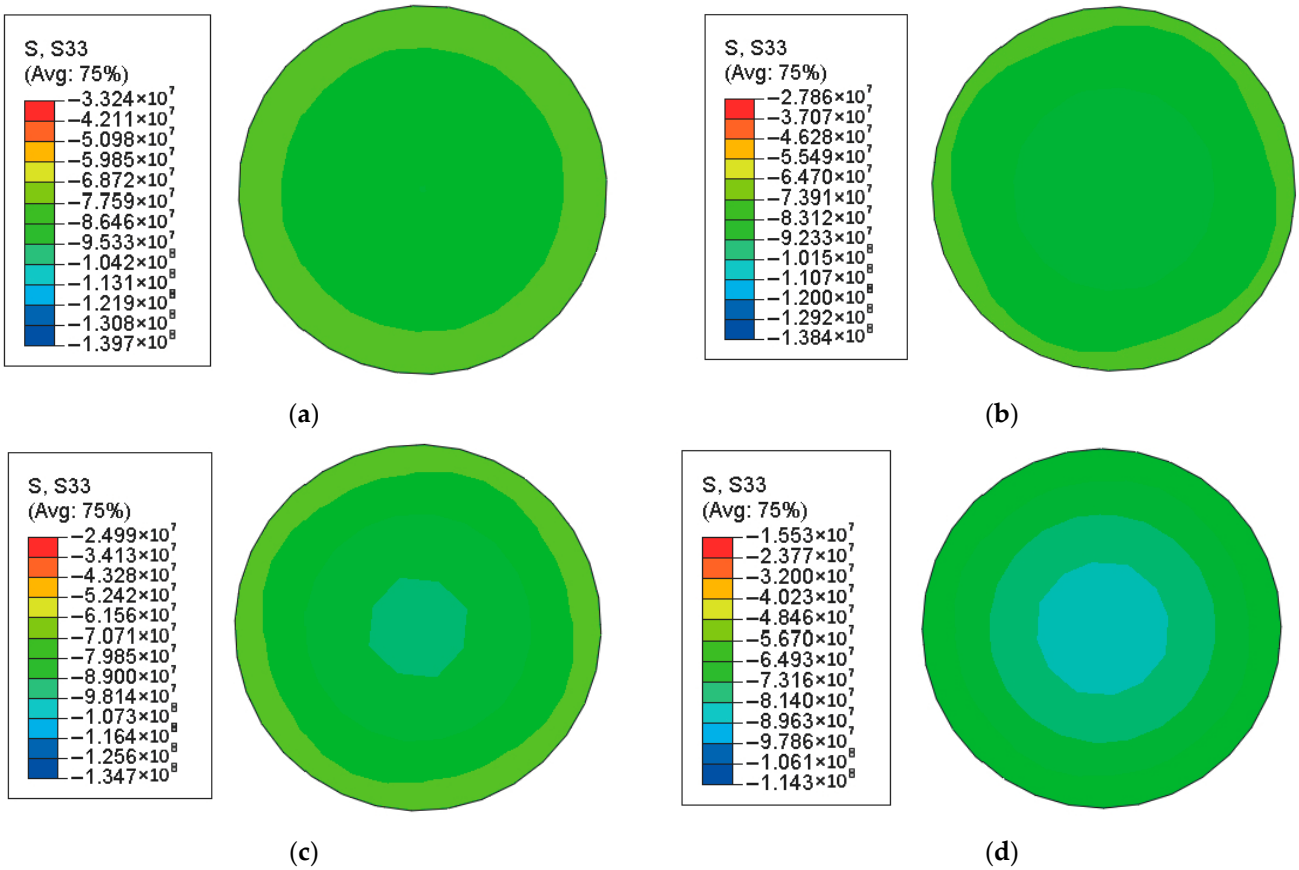



**Figure 7.** Longitudinal stress distribution of core concrete with different chloride corrosion rates in the mid-height section at point C. (**a**) C-T2-00; (**b**) C-T2-10; (**c**) C-T2-20; (**d**) C-T2-30.

#### 3.3.2. Steel Tube

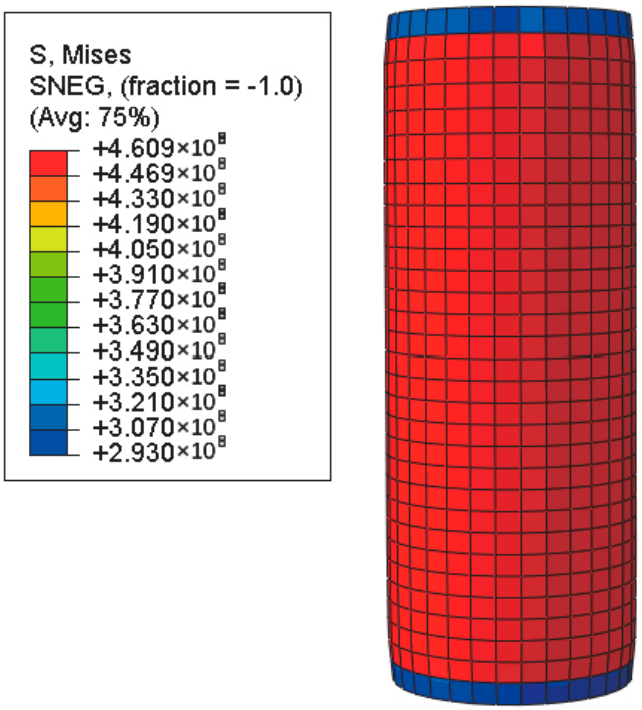
Figures 8–10 represent the Mises stress distribution of steel tubes with different corrosion rates at different characteristic loading stages (point A, point B, and point C). At point A (the end of the elastic stage), the stress distribution in the longitudinal direction is uniform. The corrosion rate has a slight effect on the value of stress, while it has an obvious effect on the distribution pattern of the steel tube in the elastic stage.

The peak longitudinal stresses of the steel tubes are 460.5 MPa, 429.2 MPa, 397.0 MPa, and 364.9 MPa corresponding to the corrosion rate of 0%, 10%, 20%, and 30%. Notably, these maximum stresses remain beneath the yield strength of the steel tube, indicating that the column is within the elastic stage. Moreover, the longitudinal stress decreases by 6.80%, 13.79%, and 20.76% with the corrosion rate increasing from 0% to 10%, 20%, and 30%, indicating that chloride corrosion has an obvious effect on the longitudinal stress of concrete, which decreases with the increasing corrosion rate.

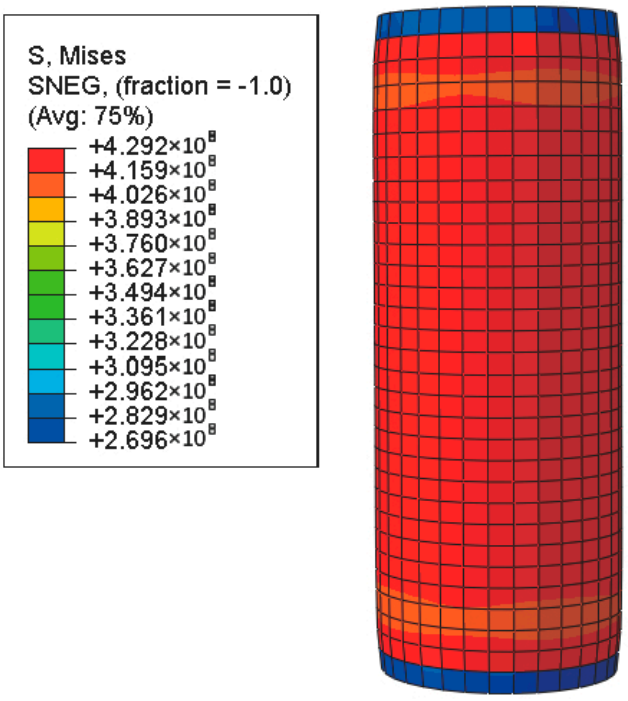
At point B (peak load), the longitudinal stresses of the steel tubes increase, compared to those at point A, as shown in Figure 9. It is evident that the chloride corrosion has a slight effect on the stress distribution of the steel tubes. The maximum longitudinal stresses are 467.8 MPa, 436.4 MPa, 405.0 MPa, and 373.6 MPa corresponding to the corrosion rate of 0%, 10%, 20%, and 30%. The longitudinal stress changes slowly except for the end of the column, indicating that a large part of the steel tube enters the yield state when the columns reach peak load. The longitudinal stress gradually increases from the mid-height section to the end of the column, illustrating that the confinement effect is larger at the end of the column.

The longitudinal stress distribution of the steel tubes at point C (failure point) are shown in Figure 10. The maximum longitudinal stresses are 526.3 MPa, 475.5 MPa, 434.8 MPa, and 405.3 MPa corresponding to the corrosion rate of 0%, 10%, 20%, and

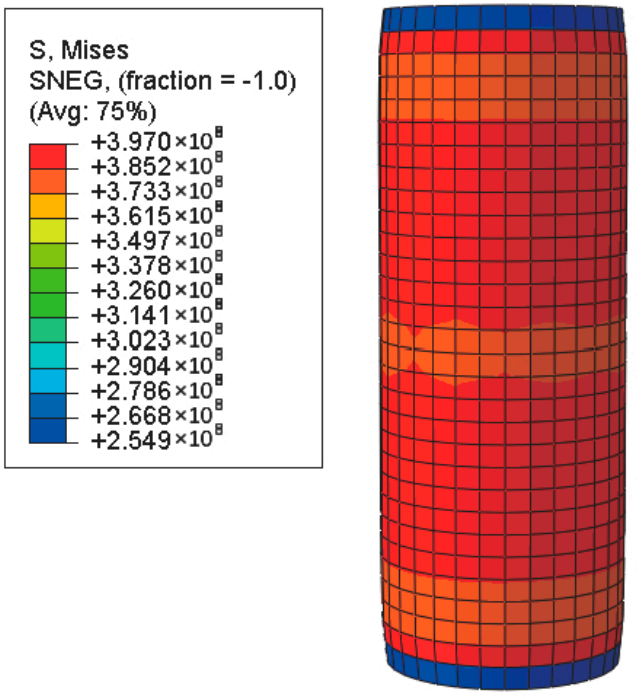
30%. During descending stage, the steel tube develops plastic behaviour. The axial load–stress curve enters the descending branch due to the increment of plastic deformation, and the confinement effect on the core concrete gradually decreases.



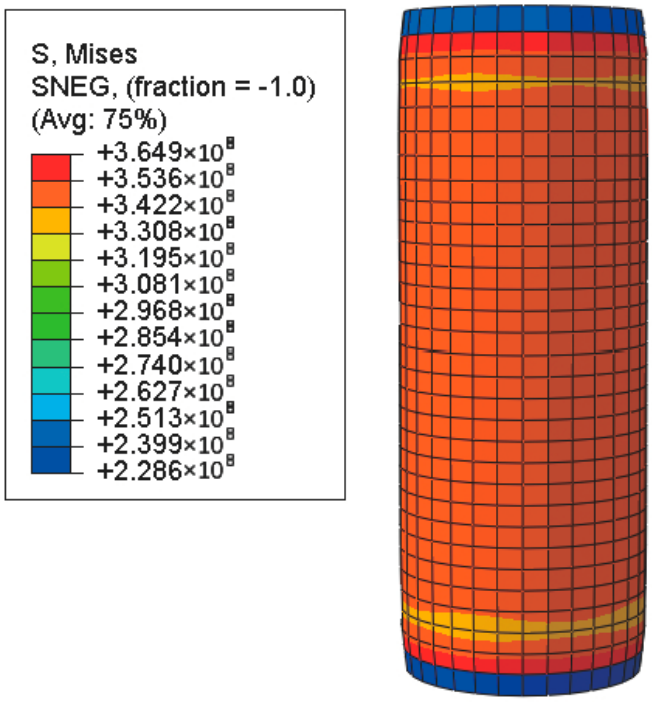

(**a**) C-T2-00




(**b**) C-T2-10

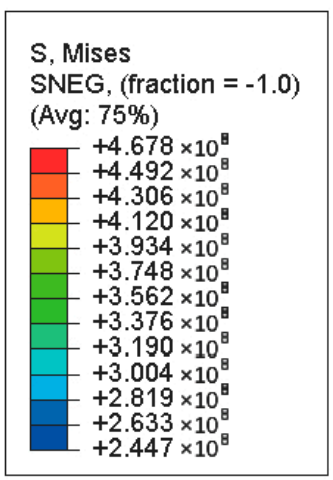


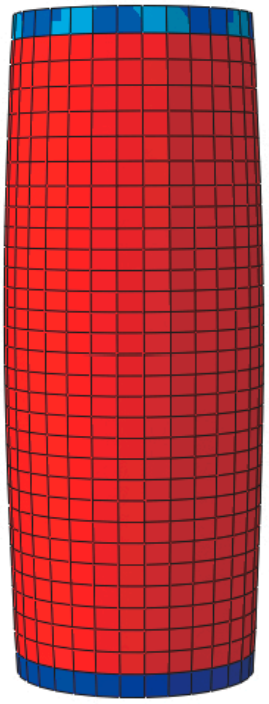

(**c**) C-T2-20



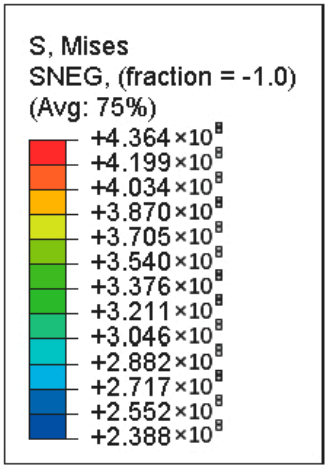

(**d**) C-T2-30

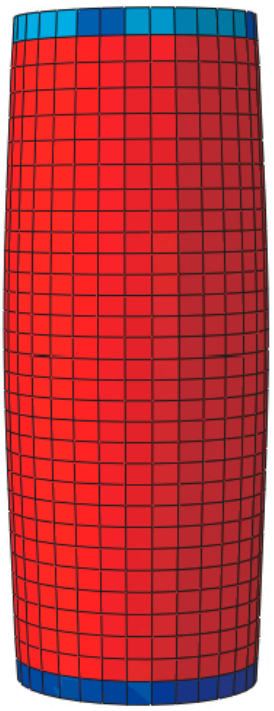
**Figure 8.** Longitudinal stress distribution of the steel tubes at point A.



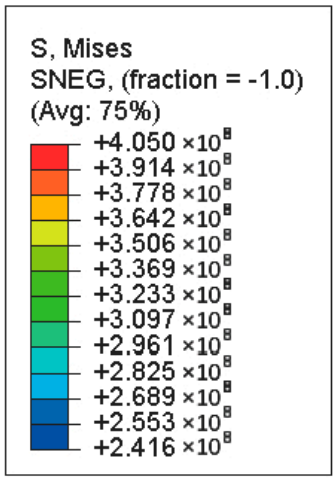



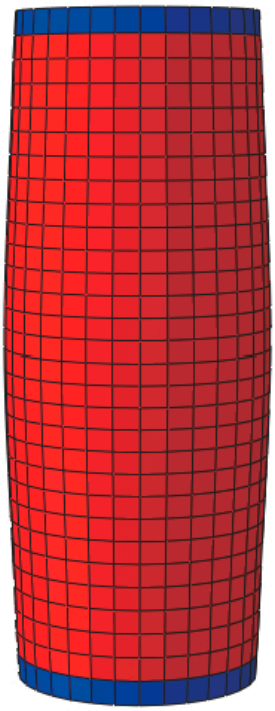
(**a**) C-T2-00



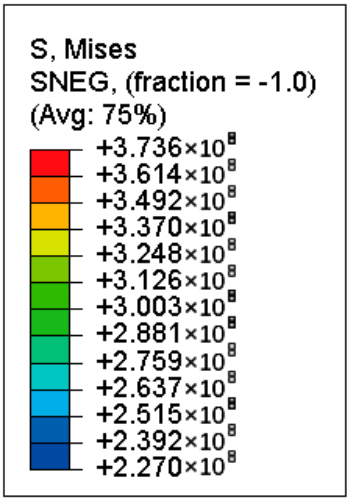



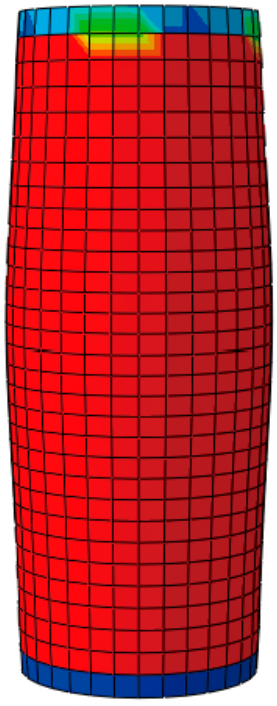
(**b**) C-T2-10



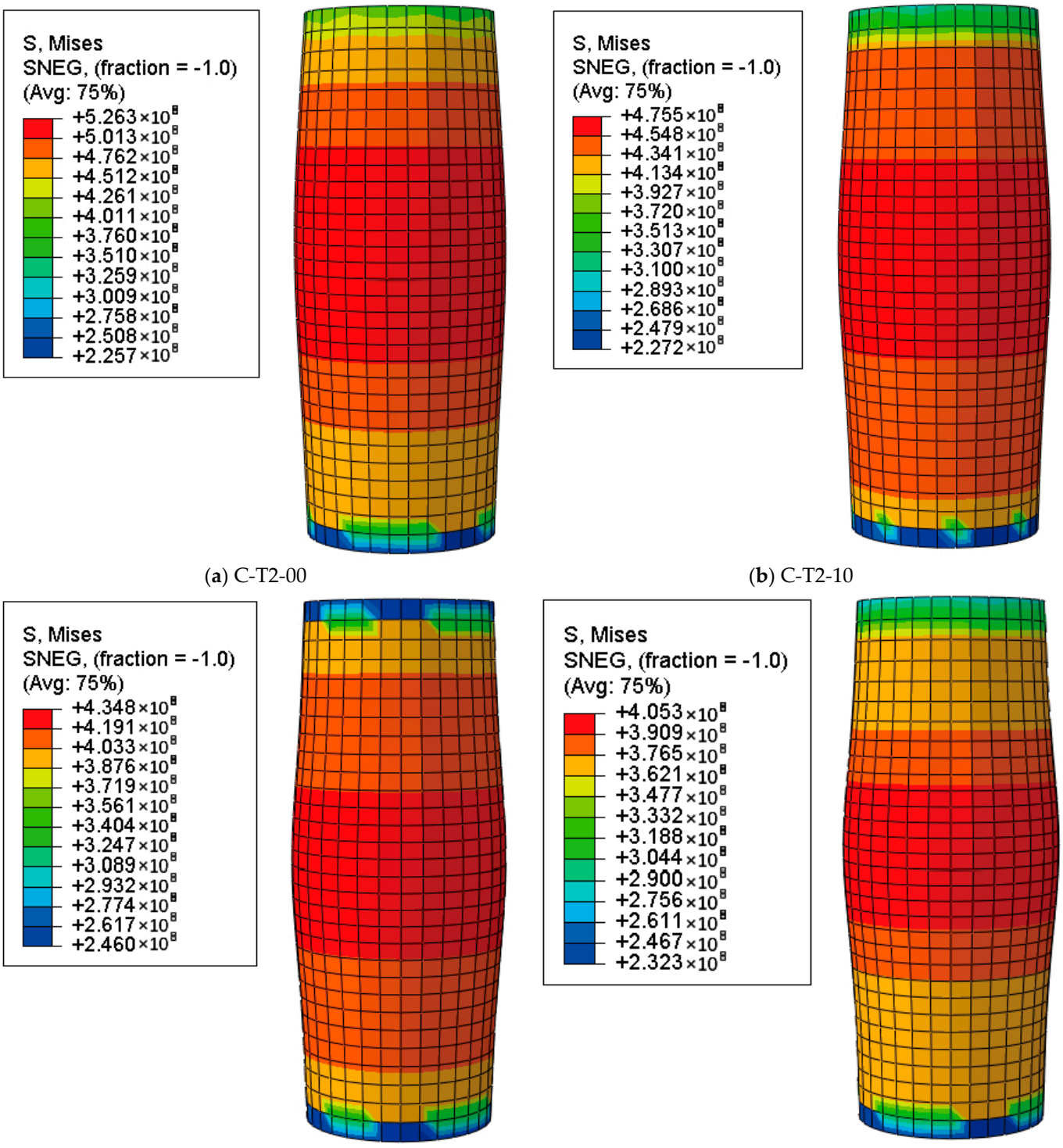
(**c**) C-T2-20



(**d**) C-T2-30

**Figure 9.** Longitudinal stress distribution of the steel tubes at point B.




(**a**) C-T2-00 (**b**) C-T2-10

(**c**) C-T2-20 (**d**) C-T2-30

**Figure 10.** Longitudinal stress distribution of the steel tubes at point C.

## 4. Parametric Investigations and Design Methods

### *4.1. Parametric Investigations*

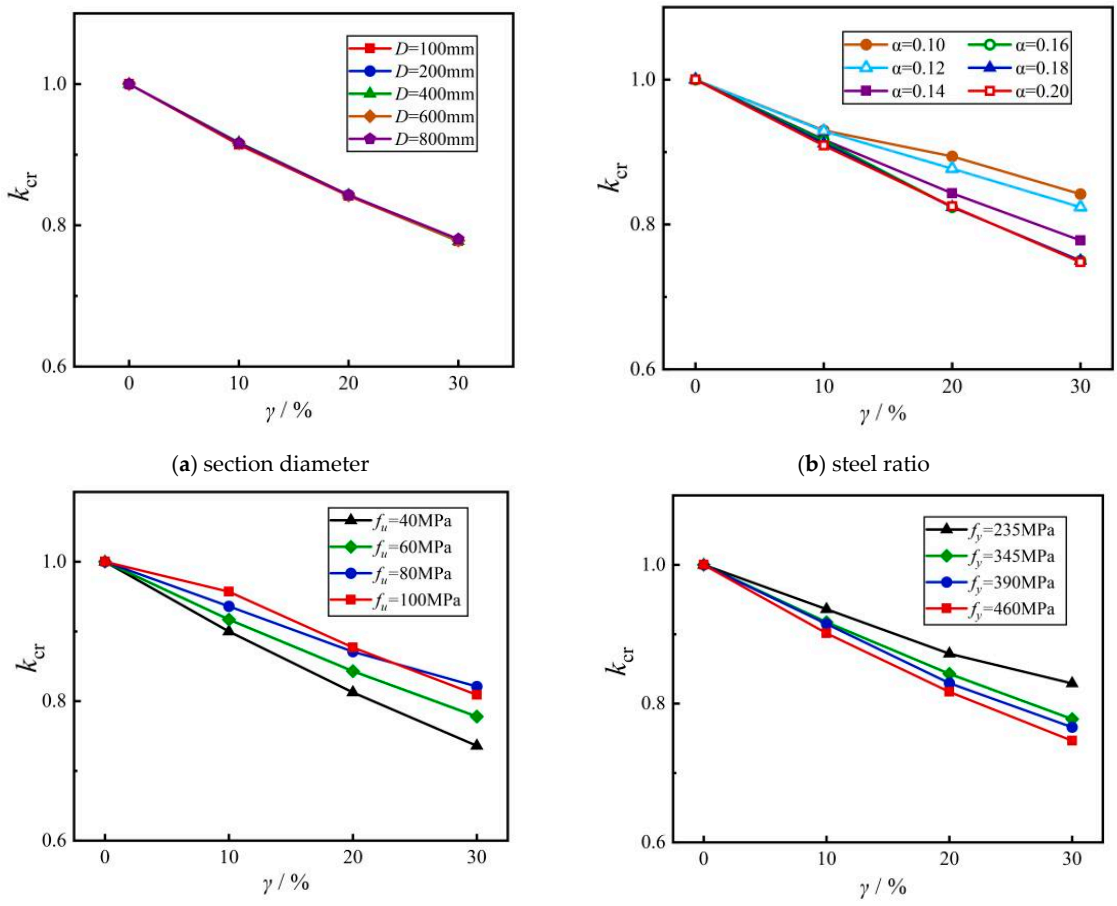
Based on validating the FE models, comprehensive parametric investigations were conducted to extend the ranges of section diameter, steel ratio, compressive strength of high-strength self-compacting concrete, yield strength of the steel tube, and corrosion rate. The parameters investigated are listed in Table 2. To study the effect of chloride

corrosion ($\gamma$) on the axial behaviour of high-strength self-compacting CFST stub columns, the standard parameter specifications of the specimen are presented in Table 2.

**Table 2.** Parametric analysis of HSSC-CFST stub columns under axial compression.

| Parameters | Ranges | Default Value |
|---|---|---|
| Section diameter $D$ (mm) | 100, 200, 400, 600, 800 | 400 |
| Steel ratio $\alpha_s$ | 0.10, 0.12, 0.14, 0.16, 0.18, 0.20 | 0.14 |
| Compressive strength of concrete $f_{cu}$ (MPa) | 40, 60, 80, 100 | 60 |
| Yield strength of the steel tube $f_y$ (MPa) | 235, 345, 390, 400 | 345 |
| Corrosion rate $\gamma$ (%) | 0, 10, 20, 30 | - |

Figure 11 shows the influences of key parameters on the ultimate compressive strength of high-strength self-compacting concrete-filled steel tubular stub columns under chloride corrosion. As presented in Figure 11a, for specimens with a steel ratio of 0.14, concrete compressive strength of 60 MPa, and steel yield strength of 345 MPa, increasing section diameter obviously affects the ultimate compressive strength of columns. In Figure 11b, for specimens with a diameter of 400 mm, concrete compressive strength of 60 MPa, and steel yield strength of 345 MPa, the residual ultimate compressive strength with different corrosion rates decreases with the increasing steel ratio. The above changes are primarily attributed to the variations in the confinement effect of the steel tube. The chloride corrosion reduces the area of the steel tube, which induces a decrease in the ultimate compressive strength of the steel tube, indicating that the steel ratio significantly affects the axial load capacity of the column.




(**a**) section diameter

(**b**) steel ratio

(**c**) compressive strength of concrete

(**d**) yield strength of the steel tube

**Figure 11.** Effect of parameters on the load-bearing capacity of high-strength self-compacting CFST stub columns.

In Figure 11c,d, the residual ultimate compressive strengths increase with an increase in the concrete compressive strength, and decrease with an increase in the yield strength of the steel tube. The strengths of the concrete and steel tube have great effects on the axial load-bearing capacities. This is mainly because the steel tube is significantly affected by the variation in the chloride rate, which deteriorates the thickness and mechanical properties of the steel tube. The increase in the concrete compressive strength induces an increase in the load-carrying capacity of the core concrete. According to the analysis of key parameters, it is structurally efficient to employ the high-strength core concrete under chloride corrosion.

### *4.2. Comparison with Current Design Codes*

To date, there exists no available design methodology for the high-strength self-compacting CFST stub columns. The design approaches outlined in EC4 [44] and ACI318 [40] are compared with both the experimental and FE results to assess their accuracy in predicting the ultimate compressive strength of the columns.

Figure 12 presents comparisons of axial load-carrying capacity of the HSSC-CFST stub columns between the calculated results in existing models and the FE results. As depicted in Figure 12, the application of the design code EC4 [44] and ACI318 [40] underestimates the axial compressive strength, thereby indicating that the confinement effect is not considered. Both EC4 and ACI318 specifications provide more conservative strength predictions. Therefore, a modification is suggested to the unified strength model which considers the confinement effect.

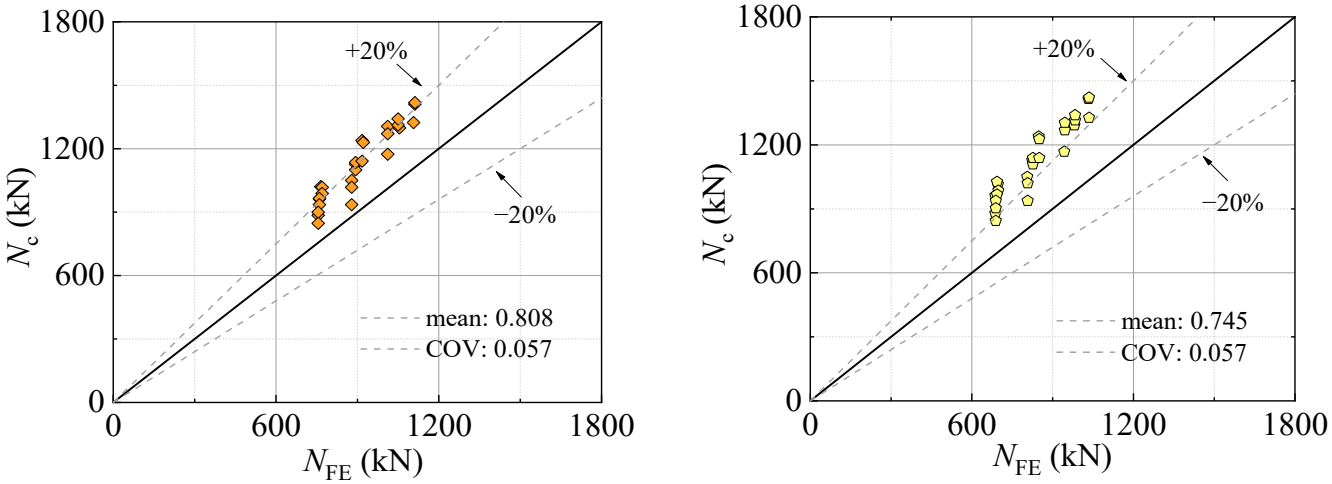



**Figure 12.** Comparison between calculated results of existing design models and FE results.

### *4.3. Design Method for Axial Compressive Strength*

Based on the thorough analysis of key parameters, it clearly shows that the reduction factor $k_{cr}$ is mainly affected by the confinement effect $\xi$, as presented in Figure 13. Thus, in this section, the proposed model is compared with the experimental and FE results to assess its applicability in high-strength self-compacting concrete-filled steel tubular stub columns, as expressed in Equation (30).

$$k_{cr} = \begin{cases} 1.0 & \gamma = 0\% \\ 0.973 - 0.049\xi_e & \gamma = 10\% \\ 0.937 - 0.105\xi_e & \gamma = 20\% \\ 0.897 - 0.163\xi_e & \gamma = 30\% \end{cases} \quad (30)$$

where $k_{cr}$ is the reduction factor of ultimate compressive strength, corresponding to the confinement coefficient subjected to chloride corrosion.

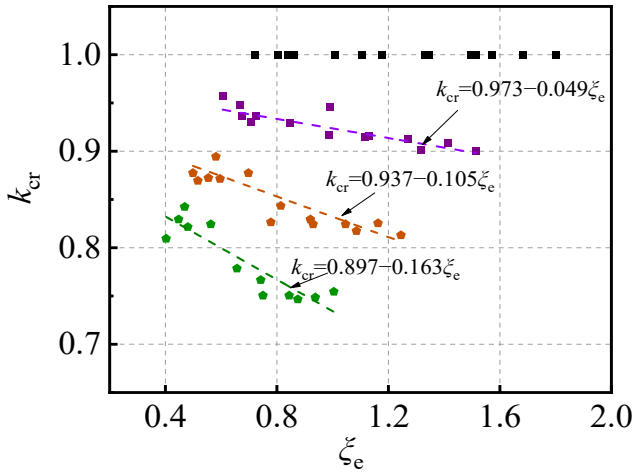



**Figure 13.** The linear regression of the $\xi_e$-$k_{cr}$ relationship.

It should be noted that the other corrosion rates below 30% can be obtained through interpolation calculation.

Since the influence of chloride corrosion on axial load-bearing capacity is factored into the reduction factor $k_{cr}$, the calculation method for the ultimate compressive strength of high-strength self-compacting concrete-filled steel tubular stub columns can be founded upon that of CFST. And it has been observed that CECS 104-99 [34] gave a comparatively accurate prediction. In this way, the axial load-bearing capacity of HSSC-CFST stub columns under chloride corrosion can be formulated as follows:

$$N_u = \begin{cases} A_c f_c (1 + \alpha_s \xi) & \xi \le \xi_\theta \\ A_c f_c \left(1 + \sqrt{\xi} + \xi\right) & \xi > \xi_\theta \end{cases} \tag{31}$$

where $N_u$ is the axial load-carrying capacity of HSSC-CFST, $A_c$ is the area of the core HSSCC, $f_c$ is the compressive strength of concrete, and $\xi$ is the confinement coefficient of HSSC-CFST subjected to chloride corrosion.

In this paper, the comparison results are presented in Figure 14. The average of the $N_{FE}/N_{cal}$ is 0.993, whereas the discrepancies between the calculation of bearing capacity and the FE results of HSSC-CFST is 0.5%. The above comparisons indicate that the calculation method by adopting Equations (30) and (31) is conservative and can be used in practical engineering structures.

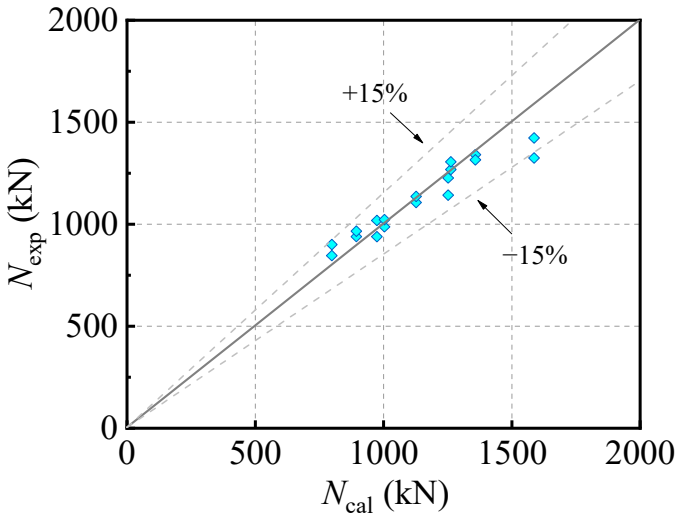



**Figure 14.** Comparison of axial load-bearing capacity between the calculated results and FE results.

## 5. Conclusions

The axial behaviour of high-strength self-compacting (HSSC) concrete-filled steel tubular (CFST) stub columns subjected to chloride corrosion is numerically investigated in this paper. FE models were established to extend the parameter ranges and predict the axial strength of specimens under chloride corrosion. The obtained FE results were used to evaluate the acceptability of existing design methods for HSSC-CFST stub columns subjected to chloride corrosion. Within the parameters of this study, the main conclusions are outlined as follows:

(1) The typical full-range axial load versus deformation curve of high-strength self-compacting concrete-filled steel tubular (HSSC-CTST) stub columns, under chloride corrosion, can be characterized by three stages: elastic stage, elastic–plastic stage, and failure stage. The ultimate compressive strength of the HSSC-CFST columns decreased by 9.60%, 16.36%, and 22.71% corresponding to the corrosion rate of 10%, 20%, and 30%, while the ultimate strain decreased by 9.09%, 15.91%, and 20.45%. The reduction of initial elastic stiffness is attributed to the deterioration of the steel tube under chloride corrosion. All stub columns failed in a ductile way, while the axial strength corresponding to failure point Ci decreased by 19.98%–34.00% with the increasing corrosion rate. It is obvious that the axial compressive behaviour of the columns decreases along with the increase in the corrosion rate.

(2) The axial load ratio carried by the steel tube decreased from 0.395 to 0.222, marking a reduction of 8.1%–41.3% corresponding to corrosion rate change from 0% to 30%. The effect of the steel tube is most pronounced on the confinement and sectional axial strength, and this effect is found to decrease with chloride corrosion. The chloride corrosion leads to a deterioration of the steel tube in mechanical properties and thickness.

(3) The parametric study results showed that the steel tube strength and steel ratio have a negative effect on the axial load-bearing capacity of columns under chloride corrosion. The compressive strength of concrete has a positive effect on the axial load-bearing capacity. The section diameter has a slight effect on the axial compressive behaviour of the HSSC-CFST stub column subjected to chloride corrosion. The confinement effect is found to be a key factor responsible for the axial load capacity. The reduction factor kcr linearly decreased with the reduction confinement coefficient $\zeta$.

(4) A modification was introduced to the axial load capacity through the reduction factor (kcr) for predicting the axial strength of HSSC-CFST stub columns subjected to different chloride corrosion rates. This was shown to predict the axial load capacity of the HSSC-CFST stub columns more accurately, which could provide theoretical reference for safety and stability evaluation and service life-time estimation of CFST specimens in corroded environments.

**Author Contributions:** J.Z.: Conceptualization, Methodology, Writing—original draft; Q.X.: Resources, Writing—review and editing, Supervision; W.W.: Validation, Writing—review and editing, Funding acquisition; Z.Z.: Software, Data curation, Writing—review and editing; M.H.: Formal analysis, Investigation, Writing—review and editing; X.L.: Conceptualization, Writing—review and editing, Project administration. All authors have read and agreed to the published version of the manuscript.

**Funding:** This research was funded by "the (Key) Project of Department of Education of Guangdong Province, grant number 2024KCXTD068", "Young Talent Innovative Project of Department of Education of Guangdong Province, grant number 2024KQNCX087" and "Doctoral Scientific Research foundation of Liaoning University of Technology, grant number XB2024026".

**Data Availability Statement:** The dataset is available on request from the corresponding author.

**Conflicts of Interest:** The authors declare no conflicts of interest.

## References

1. Han, L.H. Tests on stub columns of concrete-filled RHS sections. *J. Constr. Steel Res.* **2002**, *58*, 353–372. [CrossRef]

2. Yang, Y.F.; Han, L.H. Behaviour of concrete filled steel tubular (CFST) stub columns under eccentric partial compression. *Thin-Walled Struct.* **2011**, *49*, 379–395. [CrossRef]
3. Han, L.H.; Li, W.; Bjorhovde, R. Developments and advanced applications of concrete-filled steel tubular (CFST) structures: Member. *J. Constr. Steel Res.* **2014**, *100*, 211–228. [CrossRef]
4. Gao, F.; Zhou, H.; Liang, H.; Weng, S.; Zhu, H. Structural deformation monitoring and numerical simulation of a supertall building during construction stage. *Eng. Struct.* **2019**, *209*, 110033. [CrossRef]
5. Liu, J.P.; Teng, Y.; Zhang, Y.S.; Wang, X.D.; Chen, Y.F. Axial stress-strain behavior of high-strength concrete confined by circular thin-walled steel tubes. *Constr. Build. Mater.* **2018**, *177*, 366–377. [CrossRef]
6. Brauns, J. Analysis of stress state in concrete-filled steel column. *J. Constr. Steel Res.* **1999**, *49*, 189–196. [CrossRef]
7. Liao, Y.; Han, L.H.; He, S.H. Behavior of CFST short column and beam with initial concrete imperfection: Experiments. *J. Constr. Steel Res.* **2011**, *67*, 1922–1935. [CrossRef]
8. Chen, S.L.; Hou, C.; Zhang, H.; Han, L.H. Structural behaviour and reliability of CFST trusses with random initial imperfections. *Thin-Walled Struct.* **2019**, *143*, 106192. [CrossRef]
9. Han, L.H.; Yao, G.H. Influence of concrete compaction on the strength of concrete-filled steel RHS columns. *J. Constr. Steel Res.* **2003**, *59*, 751–767. [CrossRef]
10. Giakoumelis, G.; Lam, D. Axial capacity of circular concrete-filled tube columns. *J. Constr. Steel Res.* **2004**, *60*, 1049–1068. [CrossRef]
11. Gupta, P.K.; Sarda, S.M.; Kumar, M.S. Experimental and computational study of concrete filled steel tubular columns under axial loads. *J. Constr. Steel Res.* **2007**, *63*, 182–193. [CrossRef]
12. Saba, A.M.; Khan, A.H.; Akhtar, M.N.; Khan, N.A.; Koloor, S.S.R.; Petrů, M.; Radwan, N. Strength and flexural behavior of steel fiber and silica fume incorporated self-compacting concrete. *J. Mater. Res. Technol.* **2021**, *12*, 1380–1390. [CrossRef]
13. Lu, Y.Y.; Liu, Z.Z.; Li, S.; Li, N. Bound behavior of steel fibers reinforced self-stressing and self-compacting concrete filled steel tube columns. *Constr. Build. Mater.* **2018**, *158*, 894–909. [CrossRef]
14. Mahgub, M.; Ashour, A.; Lam, D.; Dai, X. Tests of self-compacting concrete filled elliptical steel tube columns. *Thin-Walled Struct.* **2017**, *110*, 27–34. [CrossRef]
15. Han, L.H.; Yao, G.H. Experimental behaviour of thin-walled hollow structural steel (HSS) columns filled with self-consolidating concrete (SCC). *Thin-Walled Struct.* **2004**, *42*, 1357–1377. [CrossRef]
16. Yu, Q.; Tao, Z.; Wu, Y.X. Experimental behaviour of high performance concrete-filled steel tubular columns. *Thin-Walled Struct.* **2008**, *46*, 362–370. [CrossRef]
17. Han, L.H.; Yao, G.H.; Zhao, X.L. Tests and calculations for hollow structural steel (HSS) stub columns filled with self-consolidating concrete (SCC). *J. Constr. Steel Res.* **2005**, *61*, 1241–1269. [CrossRef]
18. Ahmed, M.; Sheikh, M.N.; Muhammad, N.S.; Hadi; Liang, Q.Q. Numerical modelling of self-compacting concrete columns longitudinally reinforced with steel tubes under axial loading. *Eng. Struct.* **2022**, *270*, 114913. [CrossRef]
19. Teoh, K.B.; Chua, Y.S.; Pang, S.D.; Kong, S.Y. Experimental investigation of flexural buckling behaviour of self-compacting lightweight concrete-filled cold-formed built-up box section (CFBBS) columns. *Thin-Walled Struct.* **2023**, *187*, 110751. [CrossRef]
20. Li, N.; Lu, Y.Y.; Li, S.; Gao, D.Y. Axial compressive behaviour of steel fibre reinforced self-stressing and self-compacting concrete-filled steel tube columns. *Eng. Struct.* **2020**, *222*, 111108. [CrossRef]
21. Gong, T.N.; Xu, D.F. Seismic performance of reinforced self-compacting concrete-filled circular steel tube columns. *J. Constr. Steel Res.* **2024**, *212*, 108300. [CrossRef]
22. Ahmed, A.M.; Shaar, A.l.; Gogus, M.T. Flexural behavior of lightweight concrete and self-compacting concrete-filled steel tube beams. *J. Constr. Steel Res.* **2018**, *149*, 153–164.
23. Liao, J.J.; Li, Y.L.; Ouyang, Y.; Zeng, J.J. Axial compression tests on elliptical high strength steel tubes filled with self-compacting concrete of different mix proportions. *J. Build. Eng.* **2021**, *40*, 102678. [CrossRef]
24. Han, L.H.; Hua, Y.X.; Hou, C.; Wang, Q.L. Circular concrete-filled steel tubes subjected to coupled tension and chloride corrosion. *J. Struct. Eng.* **2017**, *143*, 04017134. [CrossRef]
25. Hou, C.; Han, L.H.; Zhao, X.L. Full-range analysis on square CFST stub columns and beams under loading and chloride corrosion. *Thin-Walled Struct.* **2013**, *68*, 50–64. [CrossRef]
26. Han, L.H.; Hou, C.C.; Wang, Q.L. Behavior of circular CFST stub columns under sustained load and chloride corrosion. *J. Constr. Steel Res.* **2014**, *103*, 23–36. [CrossRef]
27. Hou, C.C.; Han, L.H. Life-cycle performance of deteriorated concrete-filled steel tubular (CFST) structures subject to lateral impact. *Thin-Walled Struct.* **2018**, *132*, 362–374. [CrossRef]
28. Li, Y.L.; Zhao, X.L.; Raman, R.K.S.; Yu, X. Axial compression tests on seawater and sea sand concrete-filled double-skin stainless steel circular tube. *Eng. Struct.* **2018**, *176*, 426–438. [CrossRef]
29. Hua, Y.X.; Han, L.H.; Wang, Q.L.; Hou, C. Behaviour of square CFST beam-columns under combined sustained load and corrosion: Experiments. *Thin-Walled Struct.* **2019**, *136*, 353–366. [CrossRef]
30. Hua, Y.X.; Han, L.H.; Hou, C. Behaviour of square CFST beam-columns under combined sustained load and corrosion: FEA modelling and analysis. *J. Constr. Steel Res.* **2019**, *157*, 245–259. [CrossRef]
31. Guo, L.H.; Huang, H.J.; Chen, J.; Romanov, K. Axial behavior of square CFST with local corrosion simulated by artificial notch. *J. Constr. Steel Res.* **2020**, *174*, 106314. [CrossRef]

32. Lehner, P.; Kubzová, M.; Křivý, V.; Konečný, P.; Bujdoš, D.; Rovnaníková, P. Correlation between surface concentration of chloride ions and chloride deposition rate in concrete. *Constr. Build. Mater.* **2022**, *320*, 126183. [CrossRef]
33. Lehner, P.; Koubova, L.; Rosmanit, M. Study of effect of reference time of chloride diffusion coefficient in numerical modelling of durability of concrete. *Buildings* **2022**, *12*, 1443. [CrossRef]
34. *CECS104-99*; Technical Specification for High-Strength Concrete Structures. China Association for Engineering Construction Standardization (CECS): Beijing, China, 1999. (In Chinese)
35. Liu, X.J.; Yu, Z.W. Research and application of self-compacting concrete. *J. Railw. Sci. Eng.* **2006**, *3*, 6–10.
36. Yan, R. *Post-Fire Behaviors of Axially Loaded Reinforced Concrete Stub Columns Confined by Square Steel Tubes*; Harbin Institute of Technology: Harbin, China, 2017.
37. Han, L.H. *Concrete Filled Steel Tubular Structures: Theory and Practice*; China Science Press: Beijing, China, 2016. (In Chinese)
38. Zheng, Z.Y.; Lv, X.T.; Liu, X. Study on axial compressive behavior of CFRP-reinforced circular concrete-filled steel tubular stub columns subjected to chloride corrosion. *J. Foshan Univ. (Nat. Sci. Ed.)* **2022**, *40*, 41–50.
39. Chen, M.C.; Fang, W.; Huang, H.; Wang, C.; Liu, J.J. Axial compressive behavior of recycled concrete filled corroded circular steel tubular columns. *J. Build. Struct.* **2019**, *40*, 138–146.
40. *ACI318-11*; Building Code Requirements for Structural Concrete and Commentary. American Concrete Institute: Farmington Hills, MI, USA, 2011.
41. Tao, Z.; Wang, Z.B.; Yu, Q. Finite element modelling of concrete-filled steel stub columns under axial compression. *J. Constr. Steel Res.* **2013**, *89*, 121–131. [CrossRef]
42. Zheng, Z.Y. *Study on Axial Bearing Capacity of High-Strength Self-Compacting Concrete Filled Steel Tubular Piers Subjected to Chloride Corrosion*; Foshan University: Guangdong, China, 2023.
43. Li, Q. *Research on Mechanical Properties of Steel Tubular Columns Under cl Corrosion Environment*; East China Jiaotong University: Nanchang, China, 2017.
44. *EC4*; Design of Composite Steel and Concrete Structures. European Committee for Standardization: Brussels, Belgium, 2004.


**Disclaimer/Publisher's Note:** The statements, opinions and data contained in all publications are solely those of the individual author(s) and contributor(s) and not of MDPI and/or the editor(s). MDPI and/or the editor(s) disclaim responsibility for any injury to people or property resulting from any ideas, methods, instructions or products referred to in the content.